

## Rare earth element distribution in the NE Atlantic: Evidence for benthic sources, longevity of the seawater signal, and biogeochemical cycling

1 **Kirsty C. Crocket<sup>1\*</sup>, Emily Hill<sup>1§</sup>, Richard E. Abell<sup>1</sup>, Clare Johnson<sup>1</sup>, Stefan F. Gary<sup>1</sup>, Tim**  
2 **Brand<sup>1</sup>, Ed C. Hathorne<sup>2</sup>**

3 <sup>1</sup>Scottish Association for Marine Science, Scottish Marine Institute, Dunstaffnage, Argyll and Bute,  
4 UK

5 <sup>2</sup>GEOMAR Helmholtz Centre for Ocean Research, Kiel, Germany

6 <sup>§</sup>Department of Biology, Norwegian University of Science and Technology, Trondheim, Norway

7 **\*Correspondence:**

8 Kirsty C. Crocket

9 [Kirsty.crocket@sams.ac.uk](mailto:Kirsty.crocket@sams.ac.uk)

10 **Keywords: rare earths, biogeochemical cycle, ocean circulation, Northeast Atlantic, water mass**  
11 **tracer, chemical tracer, Extended Ellett Line, Iceland-Scotland Overflow Water.**  
12 **(Min.5-Max. 8)**

13 North East Atlantic, Rockall Trough, Iceland Basin, Extended Ellett Line (from 56.67 N, -6.13 E to  
14 63.32 N, -20.21 E)

15

Abstract word count: 351 (max 350)

Manuscript word count: 10197 (max 12,000)

Number of Figures and Tables: 15 (max 15 in total)

Manuscript prepared in British English.

16

17 **Abstract**

18 Seawater rare earth element (REE) concentrations are increasingly applied to reconstruct water mass  
19 histories by exploiting relative changes in the distinctive normalised patterns. However, the  
20 mechanisms by which water masses gain their patterns are yet to be fully explained. To examine this,  
21 we collected water samples along the Extended Ellett Line (EEL), an oceanographic transect between  
22 Iceland and Scotland, and measured dissolved REE by offline automated chromatography (SeaFAST)  
23 and ICP-MS. The proximity to two continental boundaries, the incipient spring bloom coincident with  
24 the timing of the cruise, and the importance of deep water circulation in this climatically sensitive  
25 gateway region make it an ideal location to investigate sources of REE to seawater and the effects of  
26 vertical cycling and lateral advection on their distribution. The deep waters have REE concentrations  
27 closest to typical North Atlantic seawater and are dominated by lateral advection. Comparison to  
28 published seawater REE concentrations of the same water masses in other locations provides a first  
29 measure of the temporal and spatial stability of the seawater REE signal. We demonstrate the REE  
30 pattern is replicated for Iceland-Scotland Overflow Water (ISOW) in the Iceland Basin from adjacent  
31 stations sampled 16 years previously. A recently published Labrador Sea Water dissolved REE signal  
32 is reproduced in the Rockall Trough but shows greater light and mid REE alteration in the Iceland  
33 Basin, possibly due to the dominant effect of ISOW and/or continental inputs. An obvious  
34 concentration gradient from seafloor sediments to the overlying water column in the Rockall Trough,  
35 but not the Iceland Basin, highlights release of light and mid REE from resuspended sediments and  
36 pore waters, possibly a seasonal effect associated with the timing of the spring bloom in each basin.  
37 The EEL dissolved oxygen minimum at the permanent pycnocline corresponds to positive heavy REE  
38 enrichment, indicating maximum rates of organic matter remineralisation and associated REE release.  
39 We tentatively suggest a bacterial role to account for the observed heavy REE deviations. This study  
40 highlights the need for fully constrained REE sources and sinks, including the temporary nature of  
41 some sources, to achieve a balanced budget of seawater REE.

42

43 **1 Introduction**

44 The rare earth elements (REE) form a suite of 14 elements (i.e. the lanthanides) with chemical  
45 properties that vary systematically across the group. The interpretation of relative changes in REE  
46 concentrations makes them a powerful tool to investigate advection, cycling and inputs of trace metals  
47 in seawater. When normalised to the Post Archaean Australian Shale (PAAS; Taylor and McLennan  
48 1985), the balance of supply/removal processes that fractionate seawater REE away from their  
49 lithogenic origins is highlighted (e.g. Elderfield and Greaves 1982, Bertram and Elderfield 1993). This  
50 fractionation is mainly attributed to the increasing strength of REE complexation to carbonate ions as  
51 mass number increases (Byrne and Kim 1990), described by the lanthanide contraction effect (Zhang  
52 and Nozaki 1996). While the heavy (H)REE are almost entirely bound by stable carbonate complexes,  
53 the light (L)REE are present with a greater proportion of free metal ions that makes them more  
54 susceptible to removal from solution through adsorption reactions (Cantrell and Byrne 1987, Byrne  
55 and Kim 1990, Sholkovitz et al. 1994). This results in the characteristic PAAS-normalised seawater  
56 REE pattern of HREE enrichment relative to LREE (e.g. Elderfield and Greaves 1982, Bertram and  
57 Elderfield 1993, Alibo and Nozaki 1999). One exception to this is Ce, whose microbially mediated  
58 redox chemistry results in substantially lower relative concentrations to neighbouring REE (Moffett  
59 1990).

60 The relative changes in the distinctive pattern of dissolved seawater REE are increasingly applied to  
61 reconstruct water mass histories, e.g. provenance, continental inputs, intensity of biogeochemical  
62 cycling, and water mass isolation time (e.g. Zhang et al. 2008, Grenier et al. 2013, Garcia-Solsona et  
63 al. 2014, Haley et al. 2014, Molina-Kescher et al. 2014, Hathorne et al. 2015, Zheng et al. 2016, Grasse  
64 et al. 2017, Grenier et al. 2018, Molina-Kescher et al. 2018). Dominant processes controlling the  
65 distribution of open ocean REE are lateral advection by deep water masses (e.g. Hathorne et al. 2015,  
66 Zheng et al. 2016) and the effects of biogeochemical cycling (particle sorption/desorption,  
67 remineralisation) on vertical profiles of REE (e.g. Sholkovitz et al. 1994). Also important are the  
68 processes operating at the continent-ocean interface, that dictate sources and sinks of REE to seawater  
69 (e.g. Jeandel et al. 2011), and, gaining recognition, are the role of organics in altering the reactivity and  
70 therefore the fractionation of the REE (Schijf et al. 2015). Demonstrating and ultimately quantifying  
71 the impact of these mechanisms on seawater REE is essential for complete data interpretation.  
72 Resolving seawater REE behaviour will also contribute to constraining the marine Nd budget (i.e. the  
73 "Nd paradox"; Goldstein and Hemming 2003), the isotope compositions of which are currently one of  
74 the most powerful chemical tracers of water masses in modern oceanography (e.g. Grenier et al. 2014,  
75 Lambelet et al. 2016) and palaeoceanographic reconstruction (e.g. Wilson et al. 2014).

76 Processes operating at continental margins and the seawater-sediment interface are amongst the least  
77 resolved. The emerging picture of REE cycling in the ocean is one of dominant removal (~70%) of  
78 riverine REE in estuaries (Goldstein and Jacobsen 1988, Sholkovitz 1993), ~20% (Nd) contribution  
79 from aeolian deposition (Tachikawa et al. 1999), negligible REE from hydrothermal venting (German  
80 et al. 1990), and variable contributions from sediments. This latter point includes diagenetic release of  
81 REE from pore waters (Abbott et al. 2015b, Haley et al. 2017), partial dissolution of particulates  
82 (Grenier et al. 2013, Pearce et al. 2013), and release from river-borne particulates in estuarine  
83 environments (Rousseau et al. 2015). These seawater-sediment interactions are described by "boundary  
84 exchange" and can result in release or scavenging of REE (Lacan and Jeandel 2005b, Jeandel et al.  
85 2007, Jeandel et al. 2011, Jeandel and Oelkers 2015, Jeandel 2016). This incomplete understanding of  
86 the marine REE budget is reflected most acutely by the input deficit in the marine Nd budget of  $\leq 1$  1000  
87 tons per year (Arsouze et al. 2009), and serves to highlight the importance of refining our knowledge  
88 of these seawater-sediment processes.

89 Organic complexation of seawater REE likely plays a role in the distribution of REE through their  
90 affinity for negatively charged sites on organic molecules (Byrne and Kim 1990). However, it remains  
91 a relatively unconstrained quantity at present (e.g. Haley et al. 2014), with some identification of  
92 organic uptake associated with surface ocean productivity (Stichel et al. 2015, Grasse et al. 2017) but  
93 no complete explanation of the process. Work on organic complexation has identified strong HREE  
94 binding to bacterial phosphate functional groups (Ngwenya et al. 2010, Takahashi et al. 2010),  
95 and strong organic ligand complexation (Schijf et al. 2015). Uptake of REE by biogenic silica has also  
96 been proposed (Akagi, 2013). Where present in sufficient density, these functional groups may serve  
97 to further fractionate seawater REE and could represent one mechanism by which the nutrient-like  
98 vertical profiles of dissolved REE are attained (Schijf et al. 2015). As rather tenuous support of this,  
99 the often cited lack of a biological function for the REE is starting to be countered by evidence for an  
100 active role of the REE in bacterial processes (Lim and Franklin, 2004, Martinez-Gomez et al. 2016,  
101 and references therein).

102 Here we present the seawater REE concentrations collected on an annual oceanographic transect, the  
103 Extended Ellett Line (EEL), which runs between Scotland and Iceland (~60 °N, ~-20 °E) and occupies  
104 a climatically sensitive gateway region in the NE Atlantic. The EEL is ideally positioned to record the  
105 influx of North Atlantic upper waters into the Greenland-Iceland-Norwegian (GIN) Seas, the overflow  
106 of deep water masses exiting the GIN Seas across the Iceland-Scotland Ridge at depth, and their  
107 recirculation within the Rockall Trough and Iceland Basin. Samples collected at five open ocean  
108 stations provide full water column REE profiles, and contribute to the growing resolution of REE  
109 distributions in water masses in the NE Atlantic, previously sampled in the neighbouring Norwegian  
110 Sea (Lacan and Jeandel 2004b), Irminger Basin (Lacan and Jeandel 2004a), Iceland Basin (Lacan and  
111 Jeandel 2005a), and Labrador Sea (Filippova et al. 2017). The comparison to data collected recently  
112 and ~16 years prior allows the first evaluation of the temporal and spatial stability of the dissolved  
113 REE signature as chemical water mass tracers. Samples were also collected from three coastal stations  
114 at the Icelandic and Scottish extremes of the EEL (Figure 1). The proximity of these two continental  
115 margins and the complex bathymetry crossed by the EEL make it an ideal location to investigate the  
116 impact of various REE sources on the seawater signatures of different water masses. In addition, the  
117 timing of the spring bloom, coincident with the EEL cruise, provides further insight into the effects of  
118 vertical biogeochemical cycling on REE distributions.

## 119 **2 Material and methods**

### 120 **2.1 Hydrography**

121 The EEL spans the Rockall Trough, the Rockall-Hatton Plateau and the Iceland Basin (Figure 1). The  
122 collection of oceanographic data on at least an annual basis since 1975 in the Rockall Trough and  
123 extended to the Iceland Basin from 1996 onwards makes the EEL an exceptional resource (Holliday  
124 and Cunningham 2013), with many publications detailing the circulation of water masses and their  
125 hydrographic and chemical properties. The overall circulation along the EEL is one of warm and salty  
126 Atlantic upper waters flowing in a north-easterly direction into the Nordic Seas, underlain by a  
127 permanent thermocline that separates the surface from the generally cyclonic circulation of dense, cold  
128 waters at depth (Holliday et al. 2015; Figures 2-3). Here, we summarise the salient points.

129 The upper waters are dominated by the North Atlantic Current (NAC) that draws in subtropical Eastern  
130 North Atlantic Water (ENAW) and subpolar Western North Atlantic Water (WNAW). Upper waters  
131 in the Rockall Trough are warmer and saltier (>9.5 °C, >35.4 salinity) compared to the Iceland Basin  
132 (>7.0 °C, >35.10 salinity; Figure 3; Holliday et al. 2000, Johnson et al. 2013). These upper ocean

133 waters have potential densities of 27.20 to 27.50 kg/m<sup>3</sup>, and are overlain by a shallow layer of  
 134 seasonally affected surface waters (<27.20 kg/m<sup>3</sup>; Holliday et al. 2015), although in 2015 water with  
 135 these densities was observed as a thin veneer over the surface of the Rockall Trough (<35 m deep) and  
 136 did not extend into the Iceland Basin (Figure 2). Typically WNAW has higher concentrations of silica  
 137 ( $\geq 7.3$   $\mu\text{mol/kg}$ ), phosphate (1.0 to 1.1  $\mu\text{mol/kg}$ ) and nitrate (14.6-15.6  $\mu\text{mol/kg}$ ), whereas the ranges in  
 138 ENAW tend to be lower (silica: 2.4-5.8  $\mu\text{mol/kg}$ , phosphate: 0.6-1.0  $\mu\text{mol/kg}$ , nitrate 10.0-12.2  
 139  $\mu\text{mol/kg}$ ; Fogelqvist et al. 2003, McGrath et al. 2012, Johnson et al. 2013). The values recorded during  
 140 EEL 2015 cruise for both upper water masses fall at the lower end or just below these ranges (Table  
 141 1), highlighting broader climate-induced changes in ocean circulation that influence nutrient  
 142 concentrations (Johnson et al. 2013).

143 The permanent thermocline forms a coherent density layer (27.50 to 27.70 kg/m<sup>3</sup>) at ~900-1400 dbar  
 144 in the Rockall Trough, but becomes broader and less well defined in the Iceland Basin where it rises  
 145 to ~400 dbar (Figure 2). The oxygen depletion zone (ODZ) and maximal nutrient concentrations are  
 146 well defined in the Rockall Trough but more diffuse in the Iceland Basin. Minimum dissolved oxygen  
 147 concentrations in the Rockall Trough during the 2015 EEL cruise were 209  $\mu\text{mol/kg}$ , with concomitant  
 148 peaks in nutrients in silica (9.8  $\mu\text{mol/kg}$ ), phosphate (1.17  $\mu\text{mol/kg}$ ) and total nitrogen (18.2  $\mu\text{mol/kg}$ ;  
 149 Table 1).

150 Below the permanent pycnocline in both basins, circulation is dominated by Labrador Sea Water  
 151 (LSW), present as a relatively homogenous body of water (3-4 °C, 34.90-34.95 salinity, 27.70 – 27.85  
 152 kg/m<sup>3</sup>; Holliday et al. 2015). Long-term observations highlight the consistently fresher and colder  
 153 properties of LSW in the Iceland Basin compared to its signature in the Rockall Trough (Holliday et  
 154 al. 2015), reflecting greater mixing along its pathway to reach the northern Rockall Trough. Typical  
 155 dissolved oxygen concentrations associated with LSW in the Rockall Trough are 260-270  $\mu\text{mol/kg}$ ,  
 156 and relatively high concentrations of silica (10.7-14.7  $\mu\text{mol/kg}$ ), phosphate (1.0-1.2  $\mu\text{mol/kg}$ ) and  
 157 nitrate (11.7-19  $\mu\text{mol/kg}$ ; Fogelqvist et al. 2003, McGrath et al. 2012, Johnson et al. 2013). During the  
 158 2015 EEL cruise, LSW identified in both the Rockall Trough and the Iceland Basin had dissolved  
 159 oxygen and nutrient concentrations within these ranges (Table 1).

160 The deepest depths of the Iceland Basin are occupied by Iceland Scotland Overflow Water (ISOW;  
 161 <3.0 °C, >27.85 kg/m<sup>3</sup>) from the Nordic Seas that enters mostly via the Faroe Bank Channel and  
 162 circulates along the western boundary of the Iceland Basin. Cyclonic recirculation results in a smaller  
 163 flow of ISOW along the eastern side of the Basin (Kanzow and Zenk 2014), likely mixed to varying  
 164 extent with the overlying LSW (Holliday et al. 2015). ISOW is well ventilated (268-286  $\mu\text{mol/kg}$ ),  
 165 with elevated concentrations of silica (9-12.6  $\mu\text{mol/kg}$ ) and nitrate (10-16  $\mu\text{mol/kg}$ ; Fogelqvist et al.  
 166 2003, McGrath et al. 2012). During the 2015 EEL cruise, ISOW had nutrient concentrations within  
 167 range of typical values, although silica was low (9.8  $\mu\text{mol/kg}$ ) and total nitrogen was high (15.3  
 168  $\mu\text{mol/kg}$ ; Table 1). Table 1 also highlights comparison to published values of ISOW (Lacan and Jeandel  
 169 2004b), collected in the Faroe Shetland Channel in 1999. Several differences to the properties of this  
 170 ISOW (e.g. lower potential temperature and salinity, greater potential density and dissolved oxygen)  
 171 can be ascribed to the effects of mixing and dilution as ISOW travels through the overflow channels  
 172 and the shallower depths of the Iceland Basin, mixing with overlying NAC and LSW. This is discussed  
 173 in more detail in Section 4.1.

174 At the point the EEL crosses the Rockall Trough, water masses denser than LSW (>27.85 kg/m<sup>3</sup>) are  
 175 not consistently observed. When present, Lower Deep Water (LDW; ~2.8 °C, 34.95 salinity; Holliday  
 176 et al. 2000) is a cold, dense water mass influenced by Antarctic Bottom Water (New and Smythe-  
 177 Wright 2001). In 2015, only the deep eastern side of the Rockall Trough carried water denser than

178 LSW (not sampled in this study), which has typical characteristics of elevated silica (35.3  $\mu\text{mol/kg}$ )  
179 and nitrate (20.4  $\mu\text{mol/kg}$ ; McGrath et al. 2013).

## 180 2.2 Methods

181 Samples were collected from nine stations during the EEL on the RRS *Discovery* between 29 May and  
182 17 June 2015 (Figure 1). Of the open ocean stations, five have full profiles (6 depths sampled) and  
183 station P has two samples. Seawater was collected from Niskin bottles on a CTD rosette and  
184 immediately filtered through 0.4  $\mu\text{m}$  polycarbonate Cyclopore filter membranes into LDPE bottles,  
185 followed by acidification, double bagging and refrigeration until analysis in the home laboratory. All  
186 equipment in contact with the sample seawater was rigorously acid cleaned prior to use (Buck and  
187 Paytan 2012, Cutter et al. 2014). Station 9G and surface samples from Station O were not filtered.

188 The REE concentrations were determined on 20 ml seawater by ICP-MS (ThermoScientific Xseries 2)  
189 following off-line preconcentration and removal of the salt matrix using a SeaFAST system (ESI,  
190 USA), adapted from the on-line method of Hathorne et al. (2012). External standardisation was applied  
191 using a 6 point calibration, the solutions of which were processed through the SeaFAST in the same  
192 manner as the samples. Calibration standards, reference seawater aliquots, and samples were indium  
193 doped to monitor and correct for instrumental drift. Oxide formation and interferences on the HREE  
194 were minimised during tuning, and monitored by measurement of mass 156 (CeO). They were found  
195 to be <1% of the 140Ce intensity for the majority of samples. The exceptions were two samples with  
196 a 156/140 ratio of ~3%. These have not been included in the dataset. Barium concentrations in the  
197 purified sample solutions were monitored for oxide interference on europium.  $^{137}\text{Ba}$  intensities were  
198 <20% of  $^{153}\text{Eu}$ , and would require >10% BaO formation to generate significant interferences on  
199 europium (i.e. >2%) and so are not considered to be significant. All data are presented in Table S1.

200 External reproducibility was determined by repeat measurement of the GEOTRACES intercalibration  
201 seawater from the Bermuda Atlantic Time Series (BATS 2000 m) and NRC NASS-6 coastal water.  
202 Over the course of this study, values ranged from 6 % to 16 % (2RSD) for the BATS and 7 % to 16 %  
203 for the NASS-6 (Table 2). Comparison of the BATS 2000 m concentrations to the consensus values  
204 (van de Flierdt et al. 2012) reveal deviations of <7 %, with the exceptions of Ce and Sm (both 14 %).  
205 We report the deviation to published values of NASS-6 (Wang et al. 2014) for information only as no  
206 certified values exist (Table 2). Duplicate samples (same Niskin vs. different Niskin/similar depth)  
207 have relative differences similar to the external reproducibility, and on a few occasions were larger.  
208 Total procedural blanks run through the preconcentration system were <1% of the average sample  
209 signal, with the exceptions of Ce and Sm that represented 17 % and 10 % respectively of the smallest  
210 sample signal.

## 211 3 Results

212 The REE concentrations show relatively small increases with depth (Figure 4, Table S1) that are  
213 atypical of open ocean profiles (e.g. De Baar et al. 1985, Alibo and Nozaki 1999, Hathorne et al. 2015).  
214 The absence of pronounced increases with depth most likely reflects the circulation of relatively young  
215 water masses, ISOW in the Iceland Basin, and LSW in both basins, and therefore the time limited  
216 accumulation of remineralised loads of dissolved REE. In addition, the relatively short water column  
217 depth (~2000 m) of the sampled stations reduces the remineralisation time of particulates and therefore  
218 the release of REE into solution. At the stations in the Rockall Trough (F, O, P), excluding the deepest  
219 samples, a relatively small spread in REE concentrations is observed (e.g. 16.2 to 21.8 pmol/kg Nd).  
220 The Iceland Basin stations (IB16, IB9) have a greater spread in REE concentrations with higher  
221 concentrations below ~1500 m ( $\leq 25.1$  pmol/kg Nd) than in the surface waters. Station IB4 on the

222 Rockall-Hatton Plateau has the reverse trend, with slightly lower concentrations at depth (~16 pmol/kg  
 223 Nd) compared to the surface (~18 pmol/kg Nd). The variation in REE concentrations at each station is  
 224 associated with clear changes in temperature, salinity, potential density, dissolved oxygen and nutrient  
 225 concentrations (Table S2; see Discussion – Lateral advection).

226 The exceptions to this pattern are the samples in the deep Rockall Trough (F, O, P) with high REE  
 227 concentrations (e.g. 43 to 60 pmol/kg Nd), where samples were collected close to the sediment surface  
 228 (<40 m above seafloor), and the coastal stations (IB22/23, 9G) with exceptionally high REE  
 229 concentrations (e.g.  $\leq 90$  pmol/kg). The coastal stations show a linear increase in REE concentration  
 230 with depth that does not correspond to the variation in beam transmission intensity (Supplementary  
 231 Information Figure 1). Furthermore, the deeper waters at 9G (unfiltered) have lower concentrations  
 232 than comparable depths at IB22/23, which were filtered. Along this part of the UK shelf, open ocean  
 233 North Atlantic water migrates onto the shelf at depth (Jones et al. 2018), supported by the high salinity  
 234 ( $\geq 35.35$ ), temperature ( $\geq 9.6$  °C) and density anomaly ( $\geq 27.27$  kg/m<sup>3</sup>) at depths below ~75 m. The low  
 235 REE concentrations in these open North Atlantic waters result in lower REE concentrations at depth at  
 236 9G compared to IB22/23. The productive shelf waters at 9G, collected in May/June, mean a component  
 237 of planktonic organisms is likely included in the sample. This is reflected by the trend towards average  
 238 marine biogenic carbonate REE in Figure 9c (see discussion in Section 4.2).

239 In contrast to the coastal stations, the REE increase at depth in the Rockall Trough appears abruptly in  
 240 the deepest samples at each station and is associated with collection from water with a high particulate  
 241 load as determined from the beam transmission data (Supplementary Information Figure 1). To note,  
 242 IB4 has the strongest decrease in beam transmission but no sample was collected from within this layer.  
 243 These samples with high REE concentrations are discussed in Section 4.2.

244 Normalisation to REE concentrations of Post-Archaean Australian Shale (PAAS) is used to  
 245 demonstrate the extent of fractionation of seawater REE from REE in the typical continental source  
 246 materials. Patterns of normalised seawater REE typically reveal HREE (e.g. Tm, Yb, Lu) enrichment  
 247 and LREE (e.g. La, Pr, Nd) depletion, due to preferential LREE removal from solution onto particles  
 248 relative to the greater stability of aqueous carbonate complexes of the HREE (Cantrell and Byrne 1987,  
 249 Byrne and Kim 1990, Sholkovitz et al. 1994). We use the PAAS values in Taylor and McLennan (1985)  
 250 to normalise the EEL data. This highlights: (i) reduced HREE enrichment in surface waters, (ii)  
 251 enrichment of all REE in deeper water masses, and (iii) exceptional MREE (e.g. Gd, Tb, Dy)  
 252 enrichment in sub-surface coastal waters (Figure 5). The lack of HREE enrichment in surface waters  
 253 relative to thermocline waters is more pronounced in the Rockall Trough than the Iceland Basin, with  
 254 the largest difference noted in the data of both the coastal stations (IB22/23, 9G). As noted above, all  
 255 the REE show increases with depth (with the exception of IB4), although the greatest spread from  
 256 surface to deep in LREE and MREE (excluding the large increases at depth at stations F, O and P) is  
 257 noted at station IB16. The coastal station data show the greatest increases in normalised REE profiles  
 258 with depth (Figure 5). The Iceland Slope (IB22/23) data have a pronounced positive Eu anomaly in the  
 259 deepest sample, reflecting the dominant mafic nature of Iceland's geology. Similar positive Eu  
 260 anomalies were identified in seawater following sediment interaction experiments using Icelandic  
 261 particulate material collected in rivers and estuaries (Pearce et al. 2013) and in seawater surrounding  
 262 Tahiti (Molina-Kescher et al. 2018).

## 263 4 Discussion

### 264 4.1 Circulation effects on REE distribution

265 Water masses along the EEL are to a certain extent related. However, the two most clearly  
 266 differentiated by source region are LSW and ISOW, originating in the North Atlantic subpolar gyre  
 267 and the Nordic Seas respectively. They are identified in the 2015 EEL data on the basis of their T/S,  
 268 density anomalies and dissolved oxygen concentrations (Figure 2, Table S2). Here we evaluate the  
 269 ability of the REE to fingerprint these water masses in the NE Atlantic and the stability of their REE  
 270 signature over time and distance by comparing to (1) a proximal record of ISOW REE collected 16  
 271 years prior to this study (Lacan and Jeandel 2004b), and (2) a distal record of deep Labrador Sea Water  
 272 (DLSW) REE collected in 2013 at the site of formation in the Labrador Sea (Filippova et al. 2017).

273 The HREE are reported in the literature as better tracers of water masses than LREE (e.g. Zheng et al.  
 274 2016) within ocean basins due to their longer residence times arising from their stronger aqueous  
 275 complexation and thus reduced particle reactivity compared to the LREE (Cantrell and Byrne 1987,  
 276 Byrne and Kim 1990). However, the limited distances and correspondingly short timescales for the  
 277 movement of these young water masses (ISOW and LSW) in the NE Atlantic in this study limits the  
 278 extent to which particle reactivity would influence the distribution of the REE (with the exception of  
 279 Ce). We therefore assume the REE behave conservatively and mainly reflect the lateral advection of  
 280 the water mass, with alteration of the REE signature chiefly attributable to mixing with other water  
 281 masses and extraneous inputs. In this section, we focus on the preformed nature of REE at depth in the  
 282 water column (below the permanent pycnocline).

### 283 *Temporal record of ISOW*

284 The ISOW data used for comparison to data in this study, expressed hereafter as pISOW, were collected  
 285 from the Faroe-Shetland Channel (Stn 23 in Figure 1) in 1999 and represent a mean of REE  
 286 concentrations in waters sampled at three depths (599 m, 800 m, 988 m; Lacan and Jeandel 2004b).  
 287 Based on potential density (Figure 2c, Figure 3c), station IB16 “sees” ISOW at depths of  $\geq 1500$  m,  
 288 while along the eastern Iceland Basin the deepest sample at IB9 (1842 m) is influenced by both ISOW  
 289 and LSW (Figure 3c). Of the two, IB16 has the strongest, least dilute signal of ISOW because it lies  
 290 immediately downstream of ISOW’s passage through the Faroe Bank Channel, with a path length  
 291 between Stn 23 and IB16 being relatively short at  $\sim 1000$  km. At IB9, ISOW lies at greater depth and  
 292 the potential density gradient with the overlying LSW is shallower indicating more diffuse recirculation  
 293 and some mixing with LSW. This is observable in Figure 3c by the greater deviation of the deep waters  
 294 towards LSW compared to IB16.

295 To test the similarity between ISOW collected in 1999 and in 2015, we first normalise REE  
 296 concentrations at IB16 (1550 m), i.e. the sample with the strongest ISOW signal (i.e.  $\sigma_\theta$  27.85 kg/m<sup>3</sup>),  
 297 by the pISOW REE concentrations. This is presented in Figure 6a and 6f (inverted light green triangles)  
 298 with a combined  $2\sigma$  external error envelope of the IB16 (1550 m) and pISOW samples. The same data  
 299 are also normalised to DLSW in Figure 6g-l for comparison. Presenting the data in this way emphasises  
 300 similarities between samples that are potentially related to the origin of the water mass. The data match  
 301 between IB16 (1550 m) and pISOW is surprisingly good, reflected by most of the pISOW-normalised  
 302 REE in the IB16 sample having a value close to unity.

303 The similarity raises the question of how discriminatory the REE are at identifying ISOW along the  
 304 EEL. For example, is the REE data match between IB16 and pISOW simply fortuitous? Normalisation  
 305 of all intermediate and deep ( $>700$  m) EEL station data by pISOW reveals clear differences between  
 306 the Iceland Basin versus the Rockall Trough and the Rockall-Hatton Plateau (Figure 6a-e). As a first  
 307 broad appraisal, these differences are ascribed to the dominant presence of LSW in the Rockall Trough  
 308 and both LSW and ISOW in the Iceland Basin.

309 A more detailed appraisal of the pISOW-normalised values within the Iceland Basin brings to attention  
 310 sample depths that lie above (IB16 1686 m) and below (IB9 1502 m) the error envelope. The higher

311 LREE and MREE concentrations observed in IB16 (1686 m) suggest interaction with sediments  
 312 (Pearce et al. 2013, Abbott et al. 2015b, Molina-Kescher et al. 2018), but this is not supported by the  
 313 beam transmission data, which do not indicate significant suspended sediment (discussed in Section  
 314 4.2). Rather the excess dissolved LREE and MREE point to sediment interaction prior to arriving at  
 315 IB16, possibly during overflow through the Faroe Shetland and Faroe Bank Channels. The sample that  
 316 lies below the error envelope (IB9 1502 m) shows greater similarity to LSW. This is expected since  
 317 waters at this depth at IB9 are largely dominated by LSW (sample  $\sigma_\theta$  of 27.76 kg/m<sup>3</sup>).

318 The shallower samples (e.g. IB16 750 m, IB9 1004 m) in the Iceland Basin also fall within the pISOW  
 319 error envelope, despite the unlikely presence of ISOW at these depths. Some of the LREE and MREE  
 320 are on the lower edge of the error envelope or below it (Nd, Sm, Eu, Gd). However, the HREE show  
 321 greater similarity to pISOW. These samples lie within the pycnocline, which is weaker in the Iceland  
 322 Basin than elsewhere on the EEL (Figure 2c), and have properties that are intermediate between surface  
 323 and deep currents (e.g. respectively  $\sigma_\theta$  of 27.61 and 27.70 kg/m<sup>3</sup>, 6.4 and 4.7 °C, 35.11 and 34.97  
 324 salinity). As the northeasterly flowing, shallower WNAW ultimately contributes to the return flow of  
 325 underlying ISOW, we would expect similarity in the HREE but a reduced match in LREE and MREE  
 326 since the higher concentrations of these in ISOW are postulated to be acquired through sediment  
 327 interaction during its return transit at depth through the Faroe-Shetland and Faroe Bank Channels. The  
 328 Iceland Basin is also an area of water recirculation and mixing, and these depths at IB16 and IB9 may  
 329 reflect the mixing of WNAW with both LSW entering the Iceland Basin from the south and ISOW as  
 330 it emerges through the Faroe Bank Channel at relatively shallow depths (sill depth of 840 m).

331 The similarity of the pISOW-normalised REE at IB9 (1842 m) is problematic in that it shows values  
 332 close to unity although the potential density of the sample ( $\sigma_\theta$  27.80 kg/m<sup>3</sup>) does not fall in the range  
 333 normally occupied by ISOW (i.e.  $\geq 27.85$  kg/m<sup>3</sup>). This deepest IB9 sample also appears to lie within  
 334 the potential temperature and salinity range of LSW (Figure 2, Figure 3). We can use mixing  
 335 proportions to identify the percentage contributions of each water mass in this sample, assuming two-  
 336 component mixing. The LREE and MREE are the most discriminatory based on the pISOW-  
 337 normalised deep DLSW of Filippova et al. (2017; Figure 6f and 6l; Table 1). The DLSW signature is  
 338 based on a mean of REE concentrations at stations 15.5 (1700 m) and 17.5 (2000 m). Taking DLSW  
 339 as unaltered LSW and IB16 (1550 m) as representative of ISOW, an average contribution can be  
 340 calculated of ~80% ISOW and ~20% DLSW in the LREE and MREE (Pr, Nd, Eu, Gd, Tb, Dy) in the  
 341 deep IB9 sample. The calculation excludes La due to similarity in concentration between ISOW at  
 342 IB16 and DLSW (see Figure 6l), and Ce because removal through oxidation makes it less reliable for  
 343 this purpose. This ratio of ~80:20 ISOW:DLSW in the REE is at odds with the mixing ratio of ~20:80  
 344 ISOW:DLSW based on the more conservative properties of potential temperature and salinity. The  
 345 disparity between the actual REE concentrations at IB9 (1842 m) and the hypothetical concentrations  
 346 based on a mixing ratio of ~20:80 ISOW:DLSW reveals the largest increases in Ce, Sm and Eu (25 to  
 347 28%), with lesser increases in the other LREE and MREE ( $\leq 11\%$ ), and HREE ( $\leq 4\%$ ). On the  
 348 assumption that two-component ISOW:DLSW mixing is an accurate reflection of the waters at IB9  
 349 (1842 m), this pattern of excess LREE and MREE points to input of a sedimentary or pore water source  
 350 to the overlying water column, discussed in more detail in Section 4.2. The beam transmission data  
 351 (Figure S1) also show evidence of suspended sediments over the bottom ~14 m. Another mechanism  
 352 to increase the REE at IB9 (1842 m), which is ~36 m above the sediment surface, is through particulate  
 353 desorption of REE in the low beam transmission zone and upward mixing. The impact of external  
 354 inputs on the distribution of seawater REE concentrations is discussed in more detail in Section 4.2.

### 355 *Distal record of LSW*

356 More generally the pISOW-normalised LREE of intermediate and deep EEL station samples lie below  
 357 the  $2\sigma$  error envelope (Figure 6a-e), except the deepest sample at each of IB16, IB9, F and O. The trend

358 for the MREE is similar, with an additional prominent Eu depletion relative to pISOW. Based on  
 359 comparison of characteristic water mass properties (Table 1), these intermediate to deep depths at all  
 360 stations are dominated by LSW, and therefore the REE patterns would not be expected to show  
 361 similarity to pISOW if they are indeed discriminatory of different water masses. This is further  
 362 reinforced when the REE concentrations in DLSW collected at source (Filippova et al. 2017) are  
 363 normalized by pISOW REE (stations 15.5 and 17.5 in Figure 1a, Figure 6f). Both this DLSW and the  
 364 LSW observed along the EEL have shared features relative to pISOW of ~15% lower LREE  
 365 concentrations (with the exception of La, which is similar in pISOW, DSLW and BATS 2000 m), fairly  
 366 prominent depletions of 50% in Ce and 30% in Eu, and steadily rising MREE to HREE concentrations  
 367 between Tb and Lu.

368 In Figure 6g-k, we normalise the deep EEL data to DLSW to provide a comparison to the other  
 369 dominant deep water mass encountered in the Iceland Basin and the Rockall Trough. The error  
 370 envelope in this case represents the combined external error of deep waters at station F (1000 – 1499  
 371 m) and DSLW (stations 15.5 and 17.5). There are clear differences between the two basins. Stations F  
 372 and O have normalised values close to unity (with the exceptions of the deepest samples), indicating  
 373 similarity to DLSW, and mostly fall within the error envelope (Fig. 6f and k). Similarities to DLSW  
 374 are also observed at IB4. At this station, the circulation pattern and origin of the deeper waters (>800  
 375 m) are not well constrained, with possible inflow across the Rockall-Hatton Plateau from either the NE  
 376 Atlantic or from overflow across the Wyville Thomson Ridge (WTR; Figure 1). The data presented  
 377 here strongly suggest an origin in the NE Atlantic and entry via the southern end of the Rockall-Hatton  
 378 Plateau. If the waters on the Rockall-Hatton Plateau were sourced from ISOW, the LREE and MREE  
 379 would be expected to have significantly higher concentrations than observed. The strong similarity  
 380 between the average deep water at station F (1000 – 1499 m) and BATS 2000 m (Fig. 6l) suggests a  
 381 common origin through mixing in the sub-polar gyre before divergence to the Rockall Trough and the  
 382 subtropical gyre respectively.

383 The clearest differences in DLSW relative to pISOW are the lower LREE and MREE concentrations,  
 384 defined by the depletions in Ce and Eu, in DLSW (Figure 6f to Figure 6l). We can explain these  
 385 differences by examining the origin of the water masses and their pathways to the point of sampling.  
 386 From the location of formation in the Labrador Sea, LSW circulates in the NE Atlantic and has less  
 387 contact than ISOW with continental margins, therefore with the marine sediments and pore waters that  
 388 carry elevated LREE and MREE in contrast to seawater REE (Abbott et al. 2015b), before arriving in  
 389 the Rockall Trough. The pISOW on the other hand, travels through narrow channels such as the Faroe-  
 390 Shetland and Faroe Bank Channels. This provides the opportunity to raise the LREE and MREE  
 391 concentrations through contact with sedimentary sources (Zhang et al. 2008, Pearce et al. 2013, Abbott  
 392 et al. 2015b), characterised by the higher Ce concentrations and also the distinctly higher Eu from the  
 393 regional mafic geology (i.e. Faroe Islands, Iceland).

#### 394 **4.2 Source of elevated REE concentrations in the deep Rockall Trough samples**

395 The REE concentrations at depth in the coastal stations (IB22/23, 9G) and the Rockall Trough (stations  
 396 F, O, P) are high (Figure 4 and Figure 5). These latter open ocean samples also diverge the most from  
 397 pISOW and DLSW (Figure 6d,e,j,k), supporting an extraneous REE contribution. No such anomaly is  
 398 observed in the Iceland Basin (IB9, IB16) or the Rockall Hatton Plateau (IB4, although no samples  
 399 were collected from within the zone of low beam transmission). The discussion in the literature on  
 400 sources of REE to the deep marine water column describes vertical scavenging by particulate REE  
 401 capture in surface waters and release at depth (e.g. Tachikawa et al. 1999, Siddall et al. 2008). A benthic  
 402 flux from pore waters to the overlying water column may also be important for the overall marine REE  
 403 budget (Elderfield and Sholkovitz 1987, Haley et al. 2004, Lacan and Jeandel 2005b, Abbott et al.

404 2015a, Abbott et al. 2015b, Haley et al. 2017), where vertical scavenging alone cannot account for  
405 deep water REE concentrations (Elderfield and Greaves 1982). Similar to the benthic flux are REE  
406 released into solution during sediment resuspension, through processes of fine particle dissolution,  
407 dissolution of labile phases adhered to the particles, and pore water release through disturbance of the  
408 sediment (Jeandel et al. 1998, Zhang and Nozaki 1998, Lacan and Jeandel 2005b, Arsouze et al. 2009,  
409 Pearce et al. 2013, Stichel et al. 2015, Grenier et al. 2018).

410 The abrupt nature of the concentration change in the deep Rockall Trough points to an upward flux  
411 rather than REE desorption from sinking particulates, which generally shows a steadier increase with  
412 depth (e.g. Hathorne et al. 2015). In addition the main deep water masses (LSW, ISOW) are young and  
413 the water column is not especially deep at the selected stations (<2000 m), reducing the influence of  
414 dissolved REE (and nutrient) accumulation through remineralisation. While advective transport is the  
415 dominant process controlling REE concentrations in the intermediate and deep ocean (Elderfield 1988,  
416 Lambelet et al. 2016, Zheng et al. 2016), the restricted nature of the Rockall Trough and its proximal  
417 location to the UK shelf mean other processes are likely to dominate (Jeandel 2016).

418 To highlight both the abrupt nature of the concentration change in the deep Rockall Trough and the  
419 influence of young water masses circulating in a relatively shallow water column (e.g. <2300 m) in the  
420 northern Rockall Trough, the ratio of increases at depth relative to surface water Nd concentrations  
421 ( $[Nd]_{depth}/[Nd]_{surface}$ ) from stations along the EEL are compared to Southern Ocean data in Hathorne  
422 et al. (2015; Figure 7). This reveals a divergence in trends below ~1000 m depth, with low relative  
423 increases with depth at the EEL stations and larger relative increases in the Southern Ocean. The  
424 exceptions are the deepest samples in the Rockall Trough that show a steep concentration gradient and  
425 an increase in Nd concentration relative to the surface waters that is similar to those observed in the  
426 Southern Ocean at ~4500 m depth.

427 The most obvious reason for the elevated REE concentrations is sample collection from depths where  
428 beam transmission is reduced (Supplementary Information Figure 1), inferring the presence of a  
429 benthic nepheloid layer and high particulate concentrations. Based on beam attenuation data, this  
430 occurs as a layer ~50 m thick above the sediment surface along UK slope (stations O and P), decreasing  
431 to <14 m in mid-Rockall Trough (F), Rockall-Hatton Plateau (IB4) and Iceland Basin (IB9), before  
432 disappearing completely in the NW Iceland Basin (IB16). Similarly elevated REE concentrations have  
433 been noted at depth in the Sagami Trough, Japan (Zhang and Nozaki 1998), and on the Mauritanian  
434 slope (Stichel et al. 2015), and attributed to REE release from resuspended slope sediments.  
435 Resuspension of sediments by currents has been noted in the Rockall Trough, where currents are strong  
436 to moderate and flow parallel to bathymetric contours (Lonsdale and Hollister 1979).

437 Zhang and Nozaki (1998) postulated that if the REE are chemical analogues to actinium, then the  
438 observed release (rather than scavenging) of actinium from slope sediments (Nozaki and Yang 1987)  
439 may also operate for the REE. In this study, the decreased beam transmission close to the seafloor  
440 confirms sediment suspension, probably driven by current action that would encourage desorption from  
441 resuspended sediments and release of associated pore waters into the overlying water column. The  
442 typically higher LREE and MREE concentrations in pore waters, relative to seawater (Abbott et al.  
443 2015b), would drive those deep waters adjacent to the seafloor to acquire REE profiles with higher  
444 LREE and MREE concentrations that deviate from typical seawater values. Release of REE from  
445 suspended particulates as the source of elevated LREE and MREE, rather than pore waters, is also  
446 possible. Here we investigate the potential of pore waters and sediment resuspension to act as a benthic  
447 source of dissolved REE to the overlying water column and evaluate the impact on seawater REE  
448 distribution.

449 *Potential sources*

450 We use the relative differences in PAAS-normalised REE concentrations (see caption to Figure 8) and  
451 their concentrations to constrain the potential sources (Figure 8). Each of the REE sources in Figure 8  
452 represents an average for clarity, and hides the range of MREE/MREE\* and HREE/LREE associated  
453 with specific phases. Both desorption from sediments and pore water release are potential candidates  
454 for the elevated REE concentrations observed in the deep water column samples. An indirect analogy  
455 is the observation of nutrient release during sediment resuspension experiments, which identified the  
456 requirement of both desorption processes and pore water release to account for the observed nutrient  
457 increases (Couceiro et al. 2013). The deepest samples with high REE concentrations show greatest  
458 similarity in the MREE/MREE\* to labile Fe phases and pore waters (Figure 8b). The relationship is  
459 less clear cut with the HREE/LREE ratio because the REE sources (labile Fe phases, sedimentary  
460 organic matter, Icelandic ash) are less well differentiated by this ratio (Figure 8c), although the data  
461 are clearly closer to the composition of these sources than typical seawater (represented by BATS 2000  
462 m and 15 m).

463 Both the MREE/MREE\* and HREE/LREE (Figure 8) show a prominent kink in the trend at ~20%  
464 height above seafloor (we present relative depth in this figure to make the coastal station data legible).  
465 This represents an artefact of the sampling depths and not the depth to which the benthic nepheloid  
466 layer influences the dissolved REE. The thickness of the decreased transmission layer ( $\leq$ ~50 m) is  
467 significantly less than ~20% height above seafloor (i.e. ~290-390 m at F, O, P). Station IB4 has the  
468 greatest decrease in beam transmission (80%) of all the stations, but no apparent influence on the REE  
469 concentrations of the deepest sample (985 m) that is located above the decreased transmission layer  
470 (top of layer is at ~1190 m). As a general observation, this suggests that the high REE concentrations  
471 observed in benthic nepheloid layers do not “leak” significant REE into the overlying water column.  
472 We observe no correlation between the thickness of the benthic nepheloid layer (or low beam  
473 transmission) and the REE concentrations of those samples collected within the layer. However, there  
474 is a correlation between the extent of beam attenuation and REE concentrations (Supplementary  
475 Information Figure 2). More detailed sampling is necessary to constrain the full extent of influence of  
476 the turbid layer on dissolved REE concentrations.

477 On the basis that the pattern of PAAS-normalised REE concentrations is indicative of the phase or  
478 source, the “excess” REE component in the deepest samples can be isolated through subtraction of the  
479 overlying water sample to reaffirm the origin of the elevated deep water concentrations (Figure 9). The  
480 Iceland Basin and Rockall-Hatton Plateau samples show no significant increase, with flat profiles and  
481 values close to zero, implying no extraneous inputs of REE at these depths and locations. The Rockall  
482 Trough and both coastal stations have positive MREE anomalies, including a prominent positive Eu  
483 anomaly for IB22/23 derived from the predominantly volcanic origin of the sediments. The “excess”  
484 component in the deep Rockall Trough and coastal samples has concentrations not dissimilar to  
485 seawater but the source of the excess REE is not discernible because the potential sources examined  
486 here have very similar PAAS normalised profiles (Figure 9b). Examination of the Y/Ho ratio (not  
487 shown) did not clarify the identification of the contributory phases. However, on the basis that pore  
488 waters are derived from a combination of Fe-rich phases, dissolution of volcanic ash, and diagenesis  
489 of organic matter, we attribute the excess REE to pore water inputs for the purposes of establishing  
490 mixing proportions.

491 *Mixing proportions*

492 Considering pore waters as the source of excess REE in the deepest water column samples, the REE  
493 composition (MREE/MREE\* and HREE/LREE) can be combined with concentration data to  
494 determine the proportional input of pore waters (Figure 10). Pore water concentrations can be highly  
495 variable, but are generally at least one order of magnitude greater than seawater REE concentrations  
496 (Elderfield and Sholkovitz 1987). In the absence of pore water REE data specific to sediments in the  
497 NE Atlantic at the time of sampling, we use the pore water concentrations from Abbott et al. (2015b),  
498 which are from a similar shelf to open ocean setting (Oregon margin, eastern North Pacific). Mixing  
499 trends are calculated between pore waters from shelf and deep ocean sediment samples, and BATS 15  
500 m and 2000 m seawater respectively, representative of seawater that is unaffected by pore water  
501 contributions in both coastal and open ocean water columns. The data are clearly differentiated between  
502 the coastal station and deep Rockall Trough samples with high concentrations, and the rest that have  
503 little apparent contribution of pore water REE (e.g.  $\sim \leq 2\%$  HREE from pore waters; Figure 10). In this  
504 instance a pore water contribution of the order of  $\sim 10\%$  for both LREE and MREE is required, relative  
505 to the BATS seawater, to account for the observed increase in the deep Rockall Trough (F, O, P) and  
506 up to 25% at the coastal stations (IB22/23, 9G), with the caveat that actual pore water REE  
507 concentrations from the sediments below the EEL may diverge from those of Abbott et al. (2015b).  
508 The higher contributions to coastal station water columns are discussed below.

509 The four water column depths represented by the pore water data of Abbott et al. (2015b) are 202 m,  
510 500 m, 1216 m, 3060 m, and they display a depth-related range of REE compositions most clearly seen  
511 in Figure 10b. The data from the deepest sites (F 1825 m, O 1953 m) form a trend defined by mixing  
512 between the deeper pore waters and BATS 2000 m seawater, and not surface ocean water (BATS 15  
513 m) and the shallowest pore water (202 m). This trend towards the deep data supports the observed  
514 variation in pore water composition reported by Abbott et al. (2015b) and suggests similar depth-  
515 related differences in pore water composition and concentration are also present in the NE Atlantic.  
516 The reasons for REE compositional gradients in pore waters are likely associated with sediment  
517 composition, reflecting the input of both different particle types and different amounts and reactivities  
518 of organic matter to the seafloor to drive diagenetic reactions, as well as current action and benthic  
519 activity that determines irrigation of the sediments and therefore contributes to the redox status of the  
520 pore waters.

521 When estimating the sedimentary REE contribution to the water column, the effect of the spring bloom  
522 on the seafloor needs to be considered. The samples in this study were collected in late May/early June  
523 during the spring bloom. This represents a period of increased transfer of organic matter to the seafloor  
524 and heightened benthic activity (e.g. Honjo and Manganini 1993, Lochte et al. 1993, Pfannkuche 1993,  
525 Rice et al. 1994, Hughes and Gage 2004). This in itself could increase the rate of transfer of REE from  
526 sediment sources to the overlying water column through bioturbation and bioirrigation. The start of the  
527 spring bloom in 2015, defined here as the time at which chlorophyll- $\alpha$  concentrations first exceed 0.5  
528  $\text{mg/m}^3$ , is identified as late April at stations F and O. This is based on satellite-reported chlorophyll- $\alpha$   
529 concentrations (<http://hermes.acri.fr/>) over the period January to July 2015, and by using mean Chl- $\alpha$   
530 at the pixel closest to the station plus the five surrounding pixels on each side ( $\pm 0.05$  latitude,  $\pm 0.075$   
531 longitude). Particulate fluxes associated with the spring bloom are pulsed and rapid, with observed  
532 particle flux transit rates of the order of 4-6 weeks (Lochte et al. 1993). The sampling of stations F and  
533 O in June 2015 may therefore have allowed sufficient time for material to reach the seafloor from a  
534 bloom initiated in late April 2015. Therefore the REE concentrations in the deep Rockall Trough  
535 observed in this study may represent a temporary or seasonal shift.

536 A further consideration, as mentioned above, is the resuspension of sediments by currents, which  
537 occurs along the slopes of the Rockall Trough (Lonsdale and Hollister 1979). Sediment resuspension

538 experiments noted significant increases in nutrient release, especially silica, attributable to pore waters,  
539 desorption and potentially microbial activity on particle surfaces (Couceiro et al. 2013). These features  
540 are notable in the silica concentrations in the deep Rockall Trough, and to a lesser extent in phosphate  
541 (Figure 11). They are possibly linked to the silica biogeochemical cycle dominated by remineralisation  
542 of diatom frustules that are hypothesised to have high REE contents (Akagi 2013). Taken together,  
543 diffusion, benthic activity and sediment resuspension may result in enhanced sedimentary REE fluxes  
544 to the water column. The seasonal aspect of the sedimentary source of REE to seawater, as a response  
545 to the spring bloom, cannot be evaluated in this study and requires further sampling either side of the  
546 spring bloom, when the diffusive flux and sediment resuspension are likely to dominate.

547 The conspicuous differences between the water column profiles of REE concentrations at the two  
548 coastal stations and the five open ocean stations can be partly attributed to effects related to water  
549 depth, e.g. <200 m vs. ~1900 m, with the caveat for station 9G samples that were not filtered. The  
550 drivers of diagenesis in the sediments are likely to be more intense on the shelf, for example the  
551 reactivity and quantity of organic matter input, the intensity of benthic activity, which shows an inverse  
552 relationship with water depth (Henderson et al. 1999), and sediment resuspension due to currents and  
553 benthic activity. To establish a quantitative evaluation of the benthic flux (i.e. the cumulative effects  
554 of diffusion, benthic activity, sediment resuspension), combined Nd isotope and REE concentration  
555 measurements are required under different seasonal conditions.

#### 556 *Implications for water mass identification*

557 One last point to mention, based on inference from the REE concentrations, is alteration of other deep  
558 water characteristics when located in the benthic nepheloid layer (or decreased beam transmission)  
559 and/or during heightened benthic activity associated with the spring bloom. The REE concentrations  
560 in those samples that lie within nepheloid layers demonstrate the influence of pore water release and/or  
561 release from suspended particulates on elevated LREE and MREE concentrations in particular. What  
562 of the other measured characteristics, e.g. nutrient and dissolved oxygen concentrations, that may also  
563 be present in different concentrations in pore waters compared to seawater? The deep Rockall Trough  
564 REE data demonstrate up to ~10 % contribution to the seawater REE load. This implies other chemical  
565 characteristics of waters in the nepheloid layer may also be shifted to higher or lower values, depending  
566 on their concentrations in pore waters, with no significant alteration in the defining properties of a  
567 water mass (i.e. temperature, salinity, potential density). All measured nutrients are present in higher  
568 concentrations in the very deepest parts of the eastern Rockall Trough, especially silica (Figure 2,  
569 Figure 11). More detailed sampling of the lower water column and direct sampling and analysis of  
570 sediment pore waters is needed to identify the influence of these on deep water characteristics.

#### 571 **4.3 Biogeochemical cycling of REE**

572 Haley et al. (2014) identified a “bio-reactive pool” of REE present in the surface ocean, characterized  
573 by noticeably lower HREE concentrations. They attributed this to the indirect effects of microbial  
574 cycling of iron, possibly as a consequence of the affinity of dissolved REE for organic molecules and  
575 ligands associated with iron reduction (Christenson and Schijf 2011). The presence of a “bio-reactive  
576 pool” goes some way to accounting for the frequently observed absence of HREE enrichment that is  
577 typical of surface ocean REE profiles (e.g. as observed in the tropical South Atlantic; Zheng et al.  
578 2016), when the expectation is the opposite; i.e. that LREE are preferentially removed from solution,  
579 compared to the HREE, due to their greater particle reactivity and also the relatively stronger  
580 solution complexation of the HREE (Cantrell and Byrne 1987, Byrne and Kim 1990, Sholkovitz et al.  
581 1994). In this section, we examine the data to determine how the pronounced decrease in dissolved

582 oxygen across the EEL relates to vertical cycling of dissolved REE between the surface ocean and the  
 583 permanent pycnocline, and if this can elucidate on the “bio-reactive pool” of REE identified by Haley  
 584 et al. (2014).

#### 585 *Oxygen Depletion Zone (ODZ)*

586 The Northeast Atlantic has an exceptionally productive annual spring bloom that results in Fe limitation  
 587 by the summer months (Nielsdottir et al. 2009). The impact of the spring bloom on the water column  
 588 can be observed in the distribution of dissolved oxygen concentrations, with a minimum at the  
 589 permanent pycnocline (Figure 2, Figure 12). This oxygen depletion zone (ODZ) is caused by particles  
 590 rich in organic matter from the surface ocean that linger and decay during their downward transit to  
 591 the seafloor. In the Rockall Trough, the ODZ is further enhanced by winter mixing that typically  
 592 reaches depths of 600 m, and therefore not as deep as the ODZ (i.e. ~800-1200 m in the Rockall  
 593 Trough), although it may reach ~1000 m in severe winters (Meincke 1986). Lateral advection at these  
 594 depths in the Rockall Trough is low (Holliday et al. 2000), implying a minimal inherited component  
 595 of dissolved REE but also a longer residence time of the water that equates to greater potential to  
 596 accumulate REE compared to elsewhere in the water column. This is not the case in the Iceland Basin,  
 597 where the ODZ is shallower and more diffuse, and hence more susceptible to obliteration by annual  
 598 winter mixing and by lateral advection. Also, at the time of sampling the spring bloom was not as well  
 599 developed in the Iceland Basin, with productivity at least ~4 times lower than in the Rockall Trough  
 600 (details below).

601 The combined effects in the Rockall Trough of remineralisation of organic matter from the annual  
 602 spring bloom, restricted winter mixing depths ( $\leq \sim 600$  m), and minimal lateral advection, likely explain  
 603 most of the marked depletion of oxygen and/or maximal apparent oxygen utilisation (AOU) values  
 604 (Figure 12) and the local maxima of nutrient concentrations (Figure 11). These have possibly  
 605 accumulated over several years until obliterated by mixing during the less frequent severe winters.  
 606 These effects are not observed in the Iceland Basin because the ODZ is shallower and within the depth  
 607 range of annual winter mixing. While the dissolved oxygen concentrations in the ODZ are not  
 608 particularly low (minimum value of  $\sim 209$   $\mu\text{mol/kg}$ ), they are superimposed on a background of much  
 609 younger, well ventilated deep waters (ISOW, LSW with  $>260$   $\mu\text{mol/kg}$ ) and the well mixed upper  
 610 water column. These features highlight the cycling of nutrients along the EEL, with removal from the  
 611 surface ocean during the spring bloom and focused remineralisation of organic matter at the permanent  
 612 pycnocline, possibly with limited annual return of the remineralised products to the surface ocean. The  
 613 influence of these processes on dissolved REE in the Rockall Trough between the surface ocean and  
 614 the permanent pycnocline is therefore dominated by biogeochemical cycling, rather than advection or  
 615 extraneous inputs.

#### 616 *Differences in REE between the surface ocean and the permanent pycnocline – concentrations and* 617 *normalised distribution patterns*

618 At each of the five open ocean stations, we took the REE sample with the lowest oxygen concentration  
 619 in the profile and subtracted the surface water REE to highlight inputs or accumulations of REE due to  
 620 remineralisation at the permanent pycnocline. The PAAS-normalised REE concentrations in the  
 621 surface and ODZ samples at stations F and O are shown in Figure 13c. To note, the surface samples at  
 622 O were not filtered. The surface water REE are the very shallowest samples in the dataset, i.e. within  
 623 12 m of the surface. In the Rockall Trough, these correspond to the thin veneer ( $<35$  m) of seasonally  
 624 affected waters ( $\geq 10.5$   $^{\circ}\text{C}$ ,  $\sigma_{\theta} < 27.16$   $\text{kg/m}^3$ ), whereas in the Iceland Basin colder and denser waters  
 625 outcropped at the surface ( $8.3$   $^{\circ}\text{C}$ ,  $\sigma_{\theta} 27.34$ - $27.38$   $\text{kg/m}^3$ ) at the time of sampling.

626 We restrict this comparison to stations F and O, because the Iceland Basin and Rockall-Hatton Plateau  
627 did not demonstrate any significant trends. The (ODZ-surface) REE signal of these stations show a  
628 depletion in Ce and fairly flat normalised profiles, with up to ~10% higher REE concentrations at the  
629 ODZ than the surface ocean. The absence of a strong remineralisation signal is attributed to the  
630 shallower depth of the ODZ in the Iceland Basin and Rockall-Hatton Plateau and the greater frequency  
631 with which winter mixing obliterates the annual accumulation of remineralised products. The  
632 accumulation of REE, therefore, is less pronounced than in the Rockall Trough.

### 633 *Biogeochemical cycling of HREE in the Rockall Trough*

634 The key feature of the (ODZ-surface) data at stations F and O is the nuanced increase in the HREE  
635 concentrations at the ODZ relative to the surface ocean (Figure 13b). The depletion in surface ocean  
636 HREE and the gain in HREE at the permanent pycnocline requires a mechanism that specifically  
637 targets surface water HREE complexation and removal to the pycnocline. An increasing body of work  
638 has identified the external complexation of HREE by functional groups on bacterial cell walls (e.g.  
639 Takahashi et al. 2005, Takahashi et al. 2007, Ngwenya et al. 2009, Ngwenya et al. 2010, Takahashi et  
640 al. 2010), the partitioning behaviour of which is illustrated in Figure 13a. The HREE enrichment  
641 observed on bacteria cell walls is due to the strong binding by multiple phosphate sites (Takahashi et  
642 al. 2010), which is not as marked in the other REE. The relative increase in partitioning with increasing  
643 atomic mass can be interpreted as an indicator of bacterial activity. In this case, the (ODZ-surface) data  
644 and the bacteria/water partition coefficients have striking similarities (Figure 13), and suggest  
645 biogeochemical cycling of HREE by bacteria in the water column.

646 It is noted that fish milt accomplishes a very similar effect by an almost identical mechanism to  
647 bacteria, with preferential HREE complexation to external phosphate functional groups confirmed in  
648 salmon milt (Takahashi et al. 2014). Fish milt is also likely to be present in the pelagic waters of the  
649 Rockall Trough (e.g. blue whiting are known to spawn in this region, Hátún et al. 2009). We cannot  
650 differentiate between these two possible agents of HREE depletion, but the end result is likely to be  
651 the same with either process, i.e. the preferential complexation and removal from solution of dissolved  
652 HREE. Fish milt, if not converted into fish spawn, is likely consumed, excreted and exported out of  
653 the surface waters. Overall, the greater body of evidence for the rapid increases in the bacterial  
654 population during the spring bloom (discussed below) and the similarities in ODZ HREE enrichment  
655 to seawater/bacteria REE partitioning behaviour suggest bacterial cycling may be a significant process.

656 In support of a bacterioplanktonic origin of the relative HREE enrichment at the ODZ, previous studies  
657 of the North Atlantic spring bloom have identified a significant and highly variable population of  
658 bacteria associated with the development of the bloom (Ducklow et al. 1993), showing a five-fold  
659 increase after initiation of the bloom that constitutes 20 to 30 % of the particulate organic carbon in the  
660 surface waters (<50 m). We tentatively propose that the (ODZ-surface) HREE signature observed in  
661 this study reflects external sorption of HREE on bacteria in the surface waters, removal of the bacteria  
662 to depth by sinking organic matter, and the release of the HREE at the ODZ due to decay of the bacteria.  
663 The presence of ODZ bacteria would result in further HREE sorption at these depths. However, in this  
664 case, the bacteria would need to be smaller than the filter membrane pore size (0.4 µm) in order for the  
665 signal to be captured in the measured filtrate.

666 In summary, the (ODZ-surface) HREE signal is visible in the Rockall Trough by virtue of a  
667 combination of factors. The intensity of the spring bloom provides the organic matter that drives the  
668 increase in both the surface water and pycnocline bacterial populations. Satellite-reported chlorophyll-  
669 a concentrations (<http://hermes.acri.fr/>) in May 2015 demonstrate the difference in productivity

670 between the two basins, with higher concentrations in the surface of the Rockall Trough (2.4 and 1.5  
671  $\text{mg}/\text{m}^3$  at stations F and O) than on the Rockall-Hatton Plateau (1.0  $\text{mg}/\text{m}^3$  at IB4) or in the Iceland  
672 Basin (0.4 and 0.2  $\text{mg}/\text{m}^3$  at stations IB9 and IB16). The spring bloom also provides the source of  
673 respirable material for oxygen consumption at the pycnocline, resulting in a well-defined ODZ and  
674 nutrient maximum. Added to these features, the restricted winter mixing and minimal lateral advection  
675 at the depths of the ODZ in the Rockall Trough (described above) mean vertical cycling results in a  
676 “distillation” effect, preserving the signal of remineralisation of the REE in the waters of the  
677 pycnocline.

678 The importance of bacteria as a proportion of total biomass in the Rockall Trough during the spring  
679 bloom supports the potential extent of this process in productive surface waters. However, this needs  
680 further targeted investigation to conclusively demonstrate the role that bacterial activity plays in REE  
681 cycling, and if preferential bacterial HREE uptake/release can account for the proportionally greater  
682 increase in dissolved HREE accumulation with depth than the LREE, and ultimately the convex shape  
683 of that increase (Schijf et al. 2015).

684 As an addendum to this section about the biological effects on dissolved REE fractionation, we mention  
685 the growing evidence for REE involvement in bacterial processes (Martinez-Gomez et al. 2016, and  
686 references therein) and the recent observations of seawater LREE depletion associated with  
687 methanotrophy following the Deepwater Horizon incident (Shiller et al. 2017). The role of LREE  
688 (particularly La) in these biological processes is an active one, rather than the apparently more passive  
689 complexation of HREE by phosphate functional groups on bacterial cell or fish milt surfaces (e.g.  
690 Takahashi et al. 2010, Takahashi et al. 2014). Thus far, LREE depletions have been identified in  
691 bacteria associated with methanotrophy, and appear to be essential or superior to Ca in the catalysis of  
692 enzymes in methanotrophs (Pol et al. 2014). These and similar processes, while not significant in the  
693 surface ocean along the EEL, may potentially be relevant in the interpretation of REE variations in  
694 other locations that experience more extreme oxygen depletion or where methanotrophs and similar  
695 bacteria are abundant (Pol et al. 2014).

## 696 **5 Conclusions**

697 The two main deep water masses along the EEL, i.e. LSW and ISOW, are readily identifiable and  
698 differentiated through their LREE and MREE concentrations. The HREE are not discriminatory in this  
699 instance. The REE profile of ISOW at IB16 is remarkably similar to that of pISOW measured 16 years  
700 prior, although the physical properties of the water mass are slightly different. The REE profile of LSW  
701 across the EEL was identifiable, relative to ISOW, by its characteristically lower LREE and MREE  
702 concentrations, e.g. ~15% lower LREE, prominent depletion of Ce (50%) and Eu (30%). These  
703 discrepancies in LREE and MREE concentrations most likely reflect their different trajectories to  
704 arrive in the Iceland Basin and the Rockall Trough, with circulation of LSW in the North Atlantic  
705 relatively free of contact with continental margin sediments. By comparison ISOW experiences  
706 channelling through the Faroe-Shetland and Faroe-Bank Channels that brings it into contact with  
707 continental margin sediments and other terrigenous inputs.

708 The elevated REE concentrations observed in the deep Rockall Trough (but not the Iceland Basin) are  
709 attributed to desorption from resuspended sediments and pore water release to the overlying water  
710 column. This is based on the similarity in REE composition between the “excess” component identified  
711 in the deep samples and typical compositions of pore water REE. In addition, the base of the water  
712 column at these stations is characterised by decreased beam transmission, typically associated with  
713 suspended particulates in benthic nepheloid layers. The high REE concentrations are also possibly a

714 temporary feature as a result of enhanced bioirrigation and bioturbation in response to the heightened  
715 flux of organic matter from the surface ocean during the NE Atlantic spring bloom, already underway  
716 by the time of the cruise. An estimated  $\sim \leq 10\%$  contribution from pore waters to the overlying water  
717 column is based on mixing between typical pore water and open ocean REE compositions  
718 (MREE/MREE\* vs. HREE/LREE). The presence of high dissolved REE concentrations in regions near  
719 the seafloor in association with high suspended contents raises the question of how reliably these water  
720 masses can be characterised and identified by these, or other, (geo)properties.

721 A role for the vertical bacterial cycling of HREE is tentatively proposed based on clear similarities  
722 between the (ODZ-surface) data and seawater/bacteria partitioning behaviour. The multiple phosphate  
723 binding sites on bacterial cell walls preferentially take up dissolved HREE from the surface ocean and  
724 release the HREE into solution during focused remineralisation at the permanent pycnocline. This  
725 accounts for the HREE depletion in the highly productive surface waters of the Rockall Trough that,  
726 at the time of sampling, were experiencing the spring bloom, and also the relative increase in HREE at  
727 the permanent pycnocline. We recognise that the conditions in the Rockall Trough allow for a  
728 “distillation” effect to be preserved in the waters of the pycnocline, which may not be present  
729 elsewhere.

### 730 **6 Conflict of Interest**

731 The authors declare that the research was conducted in the absence of any commercial or financial  
732 relationships that could be construed as a potential conflict of interest.

### 733 **7 Author Contributions**

734 All authors contributed to the design of the research and the preparation and revising of the manuscript.  
735 All authors approved the final version. EH collected and processed the samples as part of her final year  
736 bachelor research project.

### 737 **8 Funding**

738 This work was supported by the Scottish Association for Marine Science (SAMS). NERC National  
739 Capability Funding for the Extended Ellett Line (R8-H12-85) supported the participation of EH, TB,  
740 and SFG on the cruise. We acknowledge the MASTS Visiting Fellowship (VF41) received from the  
741 Marine Alliance for Science and Technology for Scotland (MASTS) that funded ECH’s visit to SAMS  
742 and collaboration with KCC in summer 2014 to set up the techniques for the measurement of seawater  
743 REE. CJ and SFG received funding from the European Union’s Horizon 2020 research and innovation  
744 programme under grant agreement No 678760 (ATLAS). This output reflects only the authors’ views  
745 and the European Union cannot be held responsible for any use that may be made of the information  
746 contained therein.

### 747 **9 Acknowledgments**

748 We thank Dr Tina van de Flierdt, Imperial College London, for providing the GEOTRACES reference  
749 seawater BATS 2000 m for use in this study, and Catherine Jeandel for her editorial handling of the  
750 manuscript. We also thank the reviewers for their helpful and insightful comments. Notably we  
751 appreciate the assiduity of Reviewer 1 whose comments and observations contributed to greatly  
752 clarifying and improving the manuscript.

### 753 **10 Supplementary Material**

754 Supplementary Material attached.

755 **References**

- 756 Abbott, A. N., B. A. Haley and J. McManus (2015a). Bottoms up: Sedimentary control of the deep  
757 North Pacific Ocean's  $\epsilon\text{Nd}$  signature. *Geology* 43:11, 1035. DOI: <https://doi.org/10.1130/G37114.1>
- 758 Abbott, A. N., B. A. Haley, J. McManus and C. E. Reimers (2015b). The sedimentary flux of dissolved  
759 rare earth elements to the ocean. *Geochimica et Cosmochimica Acta* 154, 186-200. DOI:  
760 <https://doi.org/10.1016/j.gca.2015.01.010>.
- 761 Akagi, T. (2013). Rare earth element (REE)-silicic acid complexes in seawater to explain the  
762 incorporation of REEs in opal and the "leftover" REEs in surface water: New interpretation of dissolved  
763 REE distribution profiles. *Geochimica et Cosmochimica Acta* 113, 174-192. DOI:  
764 10.1016/j.gca.2013.03.014.
- 765 Alibo, D. S. and Y. Nozaki (1999). Rare earth elements in seawater: Particle association, shale-  
766 normalization, and Ce oxidation. *Geochimica et Cosmochimica Acta* 63:3-4, 363-372. DOI:  
767 10.1016/s0016-7037(98)00279-8.
- 768 Arsouze, T., J. C. Dutay, F. Lacan and C. Jeandel (2009). Reconstructing the Nd oceanic cycle using  
769 a coupled dynamical – biogeochemical model. *Biogeosciences* 6:12, 2829-2846. DOI: 10.5194/bg-6-  
770 2829-2009.
- 771 Bayon, G., C. R. German, K. W. Burton, R. W. Nesbitt and N. J. Rogers (2004). Sedimentary Fe-Mn  
772 oxyhydroxides as paleoceanographic archives and the role of aeolian flux in regulating oceanic  
773 dissolved REE. *Earth and Planetary Science Letters* 224:3-4, 477-492. DOI:  
774 <https://doi.org/10.1016/j.epsl.2004.05.033>.
- 775 Behrens, M., J. Muratli, C. Pradoux, Y. Wu, P. Boning, H.J. Brumsack, S.L. Goldstein, B. Haley, C.  
776 Jeandel, R. Paffrath, L.D. Pena, B. Schnetger, K. Pahnke (2016). Rapid and precise analysis of rare  
777 earth elements in small volumes of seawater - Method and intercomparison. *Marine Chemistry* 186,  
778 110-120. DOI: <http://dx.doi.org/10.1016/j.marchem.2016.08.006>
- 779 Bertram, C. J. and H. Elderfield (1993). The geochemical balance of the rare-earth elements and  
780 neodymium isotopes in the oceans. *Geochimica et Cosmochimica Acta* 57:9, 1957-1986. DOI:  
781 10.1016/0016-7037(93)90087-d.
- 782 Buck, C. S. and A. Paytan (2012). Evaluation of commonly used filter substrates for the measurement  
783 of aerosol trace element solubility. *Limnology and Oceanography: Methods* 10, 790-806. DOI:  
784 <http://dx.doi.org/10.4319/lom.2012.10.790>.
- 785 Byrne, R. H. and K. H. Kim (1990). Rare-earth element scavenging in seawater. *Geochimica et*  
786 *Cosmochimica Acta* 54:10, 2645-2656. DOI: [https://doi.org/10.1016/0016-7037\(90\)90002-3](https://doi.org/10.1016/0016-7037(90)90002-3).
- 787 Cantrell, K. J. and R. H. Byrne (1987). Rare-earth element complexation by carbonate and oxalate ions.  
788 *Geochimica et Cosmochimica Acta* 51:3, 597-605. DOI: 10.1016/0016-7037(87)90072-x.
- 789 Christenson, E. A. and J. Schijf (2011). Stability of YREE complexes with the trihydroxamate  
790 siderophore desferrioxamine B at seawater ionic strength. *Geochimica et Cosmochimica Acta* 75:22,  
791 7047-7062. DOI: 10.1016/j.gca.2011.09.022.
- 792 Couceiro, F., G. R. Fones, C. E. L. Thompson, P. J. Statham, D. B. Sivyver, R. Parker, B. A. Kelly-  
793 Gerreyn and C. L. Amos (2013). Impact of resuspension of cohesive sediments at the Oyster Grounds  
794 (North Sea) on nutrient exchange across the sediment-water interface. *Biogeochemistry* 113:1-3, 37-  
795 52. DOI: 10.1007/s10533-012-9710-7.

- 796 Cutter, G., P. Andersson, L. A. Codispoti, P. Croot, R. Francois, M. C. Lohan, H. Obata and M. R. van  
797 der Loeff. (2014). "Sampling and Sample-handling Protocols for GEOTRACES Cruises (Version  
798 2.0)." 2015, from <http://www.geotraces.org/images/stories/documents/intercalibration/Cookbook.pdf>.
- 799 De Baar, H. J. W., M. P. Bacon, P. G. Brewer and K. W. Bruland (1985). Rare-earth elements in the  
800 Pacific and Atlantic Oceans. *Geochimica et Cosmochimica Acta* 49:9, 1943-1959. DOI: 10.1016/0016-  
801 7037(85)90089-4.
- 802 Du, J., B. A. Haley and A. C. Mix (2016). Neodymium isotopes in authigenic phases, bottom waters  
803 and detrital sediments in the Gulf of Alaska and their implications for paleo-circulation reconstruction.  
804 *Geochimica et Cosmochimica Acta* 193, 14-35. DOI: <http://dx.doi.org/10.1016/j.gca.2016.08.005>.
- 805 Ducklow, H. W., D. L. Kirchman, H. L. Quinby, C. A. Carlson and H. G. Dam (1993). Stocks and  
806 dynamics of bacterioplankton carbon during the spring bloom in the eastern North Atlantic Ocean.  
807 *Deep Sea Research Part II: Topical Studies in Oceanography* 40:1, 245-263. DOI:  
808 [http://dx.doi.org/10.1016/0967-0645\(93\)90016-G](http://dx.doi.org/10.1016/0967-0645(93)90016-G).
- 809 Elderfield, H. (1988). The oceanic chemistry of the rare-earth elements. *Philosophical Transactions of*  
810 *the Royal Society a-Mathematical Physical and Engineering Sciences* 325:1583, 105-126. DOI:  
811 10.1098/rsta.1988.0046.
- 812 Elderfield, H. and M. J. Greaves (1982). The rare-earth elements in sea-water. *Nature* 296:5854, 214-  
813 219. DOI: 10.1038/296214a0.
- 814 Elderfield, H. and E. R. Sholkovitz (1987). Rare-earth elements in the pore waters of reducing  
815 nearshore sediments. *Earth and Planetary Science Letters* 82:3-4, 280-288. DOI:  
816 [https://doi.org/10.1016/0012-821X\(87\)90202-0](https://doi.org/10.1016/0012-821X(87)90202-0).
- 817 Filippova, A., M. Frank, M. Kienast, J. Rickli, E. Hathorne, I. M. Yashayaev and K. Pahnke (2017).  
818 Water mass circulation and weathering inputs in the Labrador Sea based on coupled Hf–Nd isotope  
819 compositions and rare earth element distributions. *Geochimica et Cosmochimica Acta* 199, 164-184.  
820 DOI: <https://doi.org/10.1016/j.gca.2016.11.024>.
- 821 Fogelqvist, E., J. Blindheim, T. Tanhua, S. Osterhus, E. Buch and F. Rey (2003). Greenland-Scotland  
822 overflow studied by hydro-chemical multivariate analysis. *Deep-Sea Research Part I-Oceanographic*  
823 *Research Papers* 50:1, 73-102. DOI: 10.1016/s0967-0637(02)00131-0.
- 824 Freslon, N., G. Bayon, S. Toucanne, S. Bermell, C. Bollinger, S. Cheron, J. Etoubleau, Y. Germain, A.  
825 Khripounoff, E. Ponzevera and M.-L. Rouget (2014). Rare earth elements and neodymium isotopes in  
826 sedimentary organic matter. *Geochimica et Cosmochimica Acta* 140, 177-198. DOI:  
827 10.1016/j.gca.2014.05.016.
- 828 Garcia-Solsona, E., C. Jeandel, M. Labatut, F. Lacan, D. Vance, V. Chavagnac and C. Pradoux (2014).  
829 Rare earth elements and Nd isotopes tracing water mass mixing and particle-seawater interactions in  
830 the SE Atlantic. *Geochimica et Cosmochimica Acta* 125, 351-372. DOI: 10.1016/j.gca.2013.10.009.
- 831 German, C. R., G. P. Klinkhammer, J. M. Edmond, A. Mitra and H. Elderfield (1990). Hydrothermal  
832 scavenging of rare-earth elements in the ocean. *Nature* 345:6275, 516-518. DOI: 10.1038/345516a0.
- 833 Goldstein, S. J. and S. Hemming (2003). Long-lived isotopic tracers in oceanography,  
834 palaeoceanography and ice-sheet dynamics. *The Oceans and Marine Chemistry: Treatise on*  
835 *Geochemistry*. D. Holland and K. K. Turekian.
- 836 Goldstein, S. J. and S. B. Jacobsen (1988). REE in the Great-Whale River Estuary, Northwest Quebec.  
837 *Earth and Planetary Science Letters* 88:3-4, 241-252. DOI: 10.1016/0012-821x(88)90081-7.

- 838 Grasse, P., L. Bosse, E. C. Hathorne, P. Böning, K. Pahnke and M. Frank (2017). Short-term variability  
 839 of dissolved rare earth elements and neodymium isotopes in the entire water column of the Panama  
 840 Basin. *Earth and Planetary Science Letters* 475:Supplement C, 242-253. DOI:  
 841 <https://doi.org/10.1016/j.epsl.2017.07.022>.
- 842 Grenier, M., E. Garcia-Solsona, N. Lemaitre, T. W. Trull, V. Bouvier, P. Nonnotte, P. van Beek, M.  
 843 Souhaut, F. Lacan and C. Jeandel (2018). Differentiating lithogenic supplies, water mass transport and  
 844 biological processes on and off the Kerguelen Plateau using rare earth element concentrations and  
 845 neodymium isotopic compositions. *Frontiers in Marine Science* tbc, tbc.
- 846 Grenier, M., C. Jeandel and S. Cravatte (2014). From the subtropics to the equator in the Southwest  
 847 Pacific: Continental material fluxes quantified using neodymium data along modeled thermocline  
 848 water pathways. *Journal of Geophysical Research-Oceans* 119:6, 3948-3966. DOI:  
 849 10.1002/2013jc009670.
- 850 Grenier, M., C. Jeandel, F. Lacan, D. Vance, C. Venchiarutti, A. Cros and S. Cravatte (2013). From  
 851 the subtropics to the central equatorial Pacific Ocean: Neodymium isotopic composition and rare earth  
 852 element concentration variations. *Journal of Geophysical Research-Oceans* 118:2, 592-618. DOI:  
 853 10.1029/2012jc008239.
- 854 Gutjahr, M., M. Frank, C. H. Stirling, V. Klemm, T. van de Flierdt and A. N. Halliday (2007). Reliable  
 855 extraction of a deepwater trace metal isotope signal from Fe–Mn oxyhydroxide coatings of marine  
 856 sediments. *Chemical Geology* 242:3–4, 351-370. DOI:  
 857 <http://dx.doi.org/10.1016/j.chemgeo.2007.03.021>.
- 858 Haley, B. A., M. Frank, E. Hathorne and N. Pisiadis (2014). Biogeochemical implications from dissolved  
 859 rare earth element and Nd isotope distributions in the Gulf of Alaska. *Geochimica et Cosmochimica*  
 860 *Acta* 126, 455-474. DOI: 10.1016/j.gca.2013.11.012.
- 861 Haley, B. A., G. P. Klinkhammer and J. McManus (2004). Rare earth elements in pore waters of marine  
 862 sediments. *Geochimica et Cosmochimica Acta* 68:6, 1265-1279. DOI: 10.1016/j.gca.2003.09.012.
- 863 Haley, B., J. Du, A.N. Abbott, and J. McManus (2017). The impact of benthic processes on rare earth  
 864 element and neodymium isotope distributions in the oceans. *Frontiers in Marine Science* 4:426. DOI:  
 865 10.3389/fmars.2017.00426.
- 866 Hathorne, E. C., B. Haley, T. Stichel, P. Grasse, M. Zieringer and M. Frank (2012). Online  
 867 preconcentration ICP-MS analysis of rare earth elements in seawater. *Geochemistry Geophysics*  
 868 *Geosystems* 13. DOI: 10.1029/2011gc003907.
- 869 Hathorne, E. C., T. Stichel, B. Brück and M. Frank (2015). Rare earth element distribution in the  
 870 Atlantic sector of the Southern Ocean: The balance between particle scavenging and vertical supply.  
 871 *Marine Chemistry* 177, 157-171. DOI: Doi: 10.1016/j.marchem.2015.03.011.
- 872 Hátún, H., M.R. Payne, and J.A. Jacobsen (2009). The North Atlantic subpolar gyre regulates the  
 873 spawning distribution of blue whiting (*Micromesistius poutassou*). *Canadian Journal of fisheries and*  
 874 *Aquatic Sciences* 66:5, 759-770. DOI: 10.1139/F09-037.
- 875 Henderson, G. M., F. N. Lindsay and N. C. Slowey (1999). Variation in bioturbation with water depth  
 876 on marine slopes: a study on the Little Bahamas Bank. *Marine Geology* 160:1, 105-118. DOI:  
 877 [https://doi.org/10.1016/S0025-3227\(99\)00018-3](https://doi.org/10.1016/S0025-3227(99)00018-3).
- 878 Holliday, N. P. and S. A. Cunningham (2013). The Extended Ellett Line: Discoveries from 65 years of  
 879 marine observations west of the UK. *Oceanography* 26:2, 156-163. DOI:  
 880 <http://dx.doi.org/10.5670/oceanog.2013.17>.

- 881 Holliday, N. P., S. A. Cunningham, C. Johnson, S. F. Gary, C. Griffiths, J. F. Read and T. Sherwin  
 882 (2015). Multidecadal variability of potential temperature, salinity, and transport in the eastern subpolar  
 883 North Atlantic. *Journal of Geophysical Research: Oceans* 120:9, 5945-5967. DOI:  
 884 10.1002/2015JC010762.
- 885 Holliday, N. P., R. T. Pollard, J. F. Read and H. Leach (2000). Water mass properties and fluxes in the  
 886 Rockall Trough, 1975-1998. *Deep-Sea Research Part I-Oceanographic Research Papers* 47, 1303-  
 887 1332.
- 888 Honjo, S. and S. J. Manganini (1993). Annual biogenic particle fluxes to the interior of the North  
 889 Atlantic Ocean; studied at 34°N 21°W and 48°N 21°W. *Deep Sea Research Part II: Topical Studies in*  
 890 *Oceanography* 40:1, 587-607. DOI: [http://dx.doi.org/10.1016/0967-0645\(93\)90034-K](http://dx.doi.org/10.1016/0967-0645(93)90034-K).
- 891 Hughes, D. J. and J. D. Gage (2004). Benthic metazoan biomass, community structure and bioturbation  
 892 at three contrasting deep-water sites on the northwest European continental margin. *Progress in*  
 893 *Oceanography* 63:1-2, 29-55. DOI: 10.1016/j.pocean.2004.09.002.
- 894 Jeandel, C. (2016). Overview of the mechanisms that could explain the ‘Boundary Exchange’ at the  
 895 land–ocean contact. *Philosophical Transactions of the Royal Society A: Mathematical, Physical and*  
 896 *Engineering Sciences* 374:2081. DOI: 10.1098/rsta.2015.0287.
- 897 Jeandel, C., T. Arsouze, F. Lacan, P. Techine and J. C. Dutay (2007). Isotopic Nd compositions and  
 898 concentrations of the lithogenic inputs into the ocean: A compilation, with an emphasis on the margins.  
 899 *Chemical Geology* 239:1-2, 156-164.
- 900 Jeandel, C. and E. H. Oelkers (2015). The influence of terrigenous particulate material dissolution on  
 901 ocean chemistry and global element cycles. *Chemical Geology* 395:0, 50-66. DOI:  
 902 <http://dx.doi.org/10.1016/j.chemgeo.2014.12.001>.
- 903 Jeandel, C., B. Peucker-Ehrenbrink, M. T. Jones, C. R. Pearce, E. H. Oelkers, Y. Godderis, F. Lacan,  
 904 O. Aumont and T. Arsouze (2011). Ocean margins: The missing term in oceanic element budgets? *Eos,*  
 905 *Transactions American Geophysical Union* 92:26, 217-218. DOI: 10.1029/2011EO260001.
- 906 Jeandel, C., D. Thouron and M. Fieux (1998). Concentrations and isotopic compositions of neodymium  
 907 in the eastern Indian Ocean and Indonesian straits. *Geochimica et Cosmochimica Acta* 62:15, 2597-  
 908 2607. DOI: 10.1016/s0016-7037(98)00169-0.
- 909 Johnson, C., M. Inall and S. Haekkinen (2013). Declining nutrient concentrations in the northeast  
 910 Atlantic as a result of a weakening Subpolar Gyre. *Deep-Sea Research Part I-Oceanographic Research*  
 911 *Papers* 82, 95-107. DOI: 10.1016/j.dsr.2013.08.007.
- 912 Jones, S. M., F. R. Cottier, M. Inall and C. Griffiths (2018). Decadal variability on the Northwest  
 913 European continental shelf. *Progress in Oceanography* 161, 131-151,  
 914 doi:10.1016/j.pocean.2018.01.012
- 915 Kanzow, T. and W. Zenk (2014). Structure and transport of the Iceland Scotland Overflow plume along  
 916 the Reykjanes Ridge in the Iceland Basin. *Deep-Sea Research Part I-Oceanographic Research Papers*  
 917 86, 82-93. DOI: 10.1016/j.dsr.2013.11.003.
- 918 Lacan, F. and C. Jeandel (2004a). Denmark Strait water circulation traced by heterogeneity in  
 919 neodymium isotopic compositions. *Deep Sea Research, Part I* 51, 71-82.
- 920 Lacan, F. and C. Jeandel (2004b). Neodymium isotopic composition and rare earth element  
 921 concentrations in the deep and intermediate Nordic Seas: Constraints on the Iceland Scotland Overflow  
 922 Water signature. *Geochemistry Geophysics Geosystems* 5, doi:10.1029/2004GC000742. DOI:  
 923 Q11006, doi:10.1029/2004GC000742.

- 924 Lacan, F. and C. Jeandel (2005a). Acquisition of the neodymium isotopic composition of the North  
925 Atlantic Deep Water. *Geochemistry Geophysics Geosystems* 6, doi:10.1029/2005GC000956. DOI:  
926 Q12008, doi:10.1029/2005GC000956, 2005.
- 927 Lacan, F. and C. Jeandel (2005b). Neodymium isotopes as a new tool for quantifying exchange fluxes  
928 at the continent-ocean interface. *Earth and Planetary Science Letters* 232:3-4, 245-257.
- 929 Lambelet, M., T. van de Flierdt, K. Crocket, M. Rehkämper, K. Kreissig, B. Coles, M. J. A. Rijkenberg,  
930 L. J. A. Gerringa, H. J. W. de Baar and R. Steinfeldt (2016). Neodymium isotopic composition and  
931 concentration in the western North Atlantic Ocean: Results from the GEOTRACES GA02 section.  
932 *Geochimica et Cosmochimica Acta* 177, 1-29. DOI: <http://dx.doi.org/10.1016/j.gca.2015.12.019>.
- 933 Lim, S. and S. J. Franklin (2004). Lanthanide-binding peptides and the enzymes that Might Have Been.  
934 *Cellular and Molecular Life Sciences* 61:17, 2184-2188. DOI: 10.1007/s00018-004-4156-2.
- 935 Lochte, K., H. W. Ducklow, M. J. R. Fasham and C. Stienen (1993). Plankton succession and carbon  
936 cycling at 47°N 20°W during the JGOFS North Atlantic Bloom Experiment. *Deep Sea Research Part*  
937 *II: Topical Studies in Oceanography* 40:1, 91-114. DOI: [http://dx.doi.org/10.1016/0967-](http://dx.doi.org/10.1016/0967-0645(93)90008-B)  
938 [0645\(93\)90008-B](http://dx.doi.org/10.1016/0967-0645(93)90008-B).
- 939 Lonsdale, P. and C. D. Hollister (1979). A near-bottom traverse of Rockall Trough: hydrographic and  
940 geologic inferences. *Oceanologica Acta* 2, 91-105.
- 941 Martinez-Gomez, N. C., H. N. Vu and E. Skovran (2016). Lanthanide Chemistry: From Coordination  
942 in Chemical Complexes Shaping Our Technology to Coordination in Enzymes Shaping Bacterial  
943 Metabolism. *Inorganic Chemistry* 55:20, 10083-10089. DOI: 10.1021/acs.inorgchem.6b00919.
- 944 McGrath, T., C. Kivimae, E. McGovern, R. R. Cave and E. Joyce (2013). Winter measurements of  
945 oceanic biogeochemical parameters in the Rockall Trough (2009-2012). *Earth System Science Data*  
946 5:2, 375-383. DOI: 10.5194/essd-5-375-2013.
- 947 McGrath, T., G. Nolan and E. McGovern (2012). Chemical characteristics of water masses in the  
948 Rockall Trough. *Deep Sea Research Part I: Oceanographic Research Papers* 61:0, 57-73. DOI:  
949 <http://dx.doi.org/10.1016/j.dsr.2011.11.007>.
- 950 Meincke, J. (1986). Convection in the oceanic waters west of Britain. *Proceedings of the Royal Society*  
951 *of Edinburgh Section B-Biological Sciences* 88, 127-139.
- 952 Moffett, J. W. (1990). Microbially mediated cerium oxidation in sea-water. *Nature* 345:6274, 421-423.  
953 DOI: 10.1038/345421a0.
- 954 Molina-Kescher, M., M. Frank and E. Hathorne (2014). South Pacific dissolved Nd isotope  
955 compositions and rare earth element distributions: Water mass mixing versus biogeochemical cycling.  
956 *Geochimica et Cosmochimica Acta* 127, 171-189. DOI: 10.1016/j.gca.2013.11.038.
- 957 Molina-Kescher, M., E.C. Hathorne, A. Osborne, M.K. Behrens, M. Kölling, K. Pahnke and M. Frank  
958 (2018). The influence of basaltic islands on the oceanic REE distribution: A case study from the  
959 Tropical South Pacific. *Frontiers in Marine Science* 5:50. DOI: 10.3389/fmars.2018.00050.
- 960 New, A. L. and D. Smythe-Wright (2001). Aspects of the circulation in the Rockall Trough.  
961 *Continental Shelf Research* 21, 777-810.
- 962 Ngwenya, B. T., M. Magennis, V. Olive, J. F. W. Mosselmans and R. M. Ellam (2010). Discrete Site  
963 Surface Complexation Constants for Lanthanide Adsorption to Bacteria As Determined by  
964 Experiments and Linear Free Energy Relationships. *Environmental Science & Technology* 44:2, 650-  
965 656. DOI: 10.1021/es9014234.

- 966 Ngwenya, B. T., J. F. W. Mosselmans, M. Magennis, K. D. Atkinson, J. Tourney, V. Olive and R. M.  
 967 Ellam (2009). Macroscopic and spectroscopic analysis of lanthanide adsorption to bacterial cells.  
 968 *Geochimica et Cosmochimica Acta* 73:11, 3134-3147. DOI: 10.1016/j.gca.2009.03.018.
- 969 Nielsdottir, M. C., C. M. Moore, R. Sanders, D. J. Hinz and E. P. Achterberg (2009). Iron limitation of  
 970 the postbloom phytoplankton communities in the Iceland Basin. *Global Biogeochemical Cycles* 23.  
 971 DOI: 10.1029/2008gb003410.
- 972 Nozaki, Y. and H.-S. Yang (1987). Th and Pa isotopes in the waters of the western margin of the Pacific  
 973 near Japan: Evidence for release of <sup>228</sup>Ra and <sup>227</sup>Ac from slope sediments. *Journal of the  
 974 Oceanographical Society of Japan* 43:4, 217-227. DOI: 10.1007/bf02109817.
- 975 Pearce, C. R., M. T. Jones, E. H. Oelkers, C. Pradoux and C. Jeandel (2013). The effect of particulate  
 976 dissolution on the neodymium (Nd) isotope and Rare Earth Element (REE) composition of seawater.  
 977 *Earth and Planetary Science Letters* 369-370:0, 138-147. DOI:  
 978 <http://dx.doi.org/10.1016/j.epsl.2013.03.023>.
- 979 Pfannkuche, O. (1993). Benthic response to the sedimentation of particulate organic matter at the  
 980 BIOTRANS station, 47°N, 20°W. *Deep Sea Research Part II: Topical Studies in Oceanography* 40:1,  
 981 135-149. DOI: [http://dx.doi.org/10.1016/0967-0645\(93\)90010-K](http://dx.doi.org/10.1016/0967-0645(93)90010-K).
- 982 Pol, A., T.R. Barends, A. Dietl, A.F. Khadem, J. Eygensteyn, M.S. Jetten, H.J. Op den Camp (2014).  
 983 Rare earth metals are essential for methanotrophic life in volcanic mudpots. *Environmental  
 984 Microbiology* 16:1, 255-265. DOI: 10.1111/1462-2920.12249.
- 985 Rice, A. L., M. H. Thurston and B. J. Bett (1994). The IOSDL Deep Seas Program - Introduction and  
 986 photographic evidence for the presence and absence of a seasonal input of phytodetritus at contrasting  
 987 abyssal sites in the Northeastern Atlantic. *Deep-Sea Research Part I-Oceanographic Research Papers*  
 988 41:9, 1305-1320. DOI: 10.1016/0967-0637(94)90099-x.
- 989 Rousseau, T. C. C., J. E. Sonke, J. Chmeleff, P. van Beek, M. Souhaut, G. Boaventura, P. Seyler and  
 990 C. Jeandel (2015). Rapid neodymium release to marine waters from lithogenic sediments in the  
 991 Amazon estuary. *Nature Communications* 6. DOI: 10.1038/ncomms8592.
- 992 Schijf, J., E. A. Christenson and R. H. Byrne (2015). YREE scavenging in seawater: A new look at an  
 993 old model. *Marine Chemistry* 177, Part 3, 460-471. DOI:  
 994 <http://dx.doi.org/10.1016/j.marchem.2015.06.010>.
- 995 Schlitzer, R. (2016). Ocean Data View.
- 996 Shiller, A.M, E.W. Chan, D.J. Jounge, M.C. Redmond, J.D. Kessler (2017). Light rare earth element  
 997 depletion during Deepwater Horizon blowout methanotrophy. *Scientific Reports* 7, Article number:  
 998 10389. DOI: 10.1038/s41598-017-11060-z.
- 999 Sholkovitz, E. and G. T. Shen (1995). The incorporation of rare earth elements in modern coral.  
 1000 *Geochimica et Cosmochimica Acta* 59:13, 2749-2756.
- 1001 Sholkovitz, E. R. (1993). The geochemistry of rare-earth elements in the Amazon River Estuary.  
 1002 *Geochimica et Cosmochimica Acta* 57:10, 2181-2190. DOI: 10.1016/0016-7037(93)90559-f.
- 1003 Sholkovitz, E. R., W. M. Landing and B. L. Lewis (1994). Ocean particle chemistry - the fractionation  
 1004 of rare-earth elements between suspended particles and seawater. *Geochimica et Cosmochimica Acta*  
 1005 58:6, 1567-1579. DOI: 10.1016/0016-7037(94)90559-2.
- 1006 Siddall, M., S. Khatiwala, T. van de Flierdt, K. Jones, S. L. Goldstein, S. Hemming and R. F. Anderson  
 1007 (2008). Towards explaining the Nd paradox using reversible scavenging in an ocean general circulation

- 1008 model. *Earth and Planetary Science Letters* 274:3–4, 448–461. DOI:  
1009 <http://dx.doi.org/10.1016/j.epsl.2008.07.044>.
- 1010 Stichel, T., A. E. Hartman, B. Duggan, S. L. Goldstein, H. Scher and K. Pahnke (2015). Separating  
1011 biogeochemical cycling of neodymium from water mass mixing in the Eastern North Atlantic. *Earth*  
1012 *and Planetary Science Letters* 412, 245–260. DOI: 10.1016/j.epsl.2014.12.008.
- 1013 Tachikawa, K., C. Jeandel and M. Roy-Barman (1999). A new approach to the Nd residence time in  
1014 the ocean: the role of atmospheric inputs. *Earth and Planetary Science Letters* 170:4, 433–446.
- 1015 Takahashi, Y., X. Chatellier, K. H. Hattori, K. Kato and D. Fortin (2005). Adsorption of rare earth  
1016 elements onto bacterial cell walls and its implication for REE sorption onto natural microbial mats.  
1017 *Chemical Geology* 219:1–4, 53–67. DOI: 10.1016/j.chemgeo.2005.02.009.
- 1018 Takahashi, Y., T. Hirata, H. Shimizu, T. Ozaki and D. Fortin (2007). A rare earth element signature of  
1019 bacteria in natural waters? *Chemical Geology* 244:3–4, 569–583. DOI:  
1020 10.1016/j.chemgeo.2007.07.005.
- 1021 Takahashi, Y., M. Yamamoto, Y. Yamamoto and K. Tanaka (2010). EXAFS study on the cause of  
1022 enrichment of heavy REEs on bacterial cell surfaces. *Geochimica et Cosmochimica Acta* 74:19, 5443–  
1023 5462. DOI: 10.1016/j.gca.2010.07.001.
- 1024 Takahashi, Y., K. Aondo, A. Miyaji, Y. Watanabe, Q. Fan, T. Honma, and K. Tanaka (2014). Recovery  
1025 and separation of rare earth elements using salmon milt. *PLoS ONE* 9:12, e114848. DOI:  
1026 10.1371/journal.pone.0114858.
- 1027 Taylor, S. R. and S. M. McLennan (1985). The Continental Crust: its composition and evolution.  
1028 Oxford, Blackwell Scientific Publishers.
- 1029 Tepe, N. and M. Bau (2014). Importance of nanoparticles and colloids from volcanic ash for riverine  
1030 transport of trace elements to the ocean: Evidence from glacial-fed rivers after the 2010 eruption of  
1031 Eyjafjallajökull Volcano, Iceland. *Science of the Total Environment* 488, 243–251. DOI:  
1032 10.1016/j.scitotenv.2014.04.083.
- 1033 van de Flierdt, T., K. Pahnke, H. Amakawa, P. Andersson, C. Basak, B. Coles, C. Colin, K. Crocket,  
1034 M. Frank, N. Frank, S. L. Goldstein, V. Goswami, B. A. Haley, E. C. Hathorne, S. R. Hemming, G.  
1035 M. Henderson, C. Jeandel, K. Jones, K. Kreissig, F. Lacan, M. Lambelet, E. E. Martin, D. R. Newkirk,  
1036 H. Obata, L. Pena, A. M. Piotrowski, C. Pradoux, H. D. Scher, H. Schoberg, S. K. Singh, T. Stichel,  
1037 H. Tazoe, D. Vance, J. J. Yang and G. I. Partici (2012). GEOTRACES intercalibration of neodymium  
1038 isotopes and rare earth element concentrations in seawater and suspended particles. Part 1:  
1039 reproducibility of results for the international intercomparison. *Limnology and Oceanography-*  
1040 *Methods* 10, 234–251. DOI: 10.4319/lom.2012.10.234.
- 1041 Wang, B.-S., C.-P. Lee and T.-Y. Ho (2014). Trace metal determination in natural waters by automated  
1042 solid phase extraction system and ICP-MS: The influence of low level Mg and Ca. *Talanta* 128, 337–  
1043 344. DOI: 10.1016/j.talanta.2014.04.077.
- 1044 Wilson, D. J., K. C. Crocket, T. van de Flierdt, L. F. Robinson and J. F. Adkins (2014). Dynamic  
1045 intermediate ocean circulation in the North Atlantic during Heinrich Stadial 1: A radiocarbon and  
1046 neodymium isotope perspective. *Paleoceanography*, 2014PA002674. DOI: 10.1002/2014PA002674.
- 1047 Zhang, J. and Y. Nozaki (1996). Rare earth elements and yttrium in seawater: ICP-MS determinations  
1048 in the East Caroline, Coral Sea, and South Fiji basins of the western South Pacific Ocean. *Geochimica*  
1049 *et Cosmochimica Acta* 60:23, 4631–4644. DOI: [http://dx.doi.org/10.1016/S0016-7037\(96\)00276-1](http://dx.doi.org/10.1016/S0016-7037(96)00276-1).

- 1050 Zhang, J. and Y. Nozaki (1998). Behavior of rare earth elements in seawater at the ocean margin: A  
1051 study along the slopes of the Sagami and Nankai troughs near Japan. *Geochimica et Cosmochimica*  
1052 *Acta* 62:8, 1307-1317. DOI: 10.1016/s0016-7037(98)00073-8.
- 1053 Zhang, Y., F. Lacan and C. Jeandel (2008). Dissolved rare earth elements tracing lithogenic inputs over  
1054 the Kerguelen Plateau (Southern Ocean). *Deep Sea Research Part II: Topical Studies in Oceanography*  
1055 55:5, 638-652. DOI: <https://doi.org/10.1016/j.dsr2.2007.12.029>.
- 1056 Zheng, X.-Y., Y. Plancherel, M. A. Saito, P. Scott and G. M. Henderson (2016). Rare earth elements  
1057 (REEs) in the tropical South Atlantic and quantitative deconvolution of their non-conservative  
1058 behaviour. *Geochimica et Cosmochimica Acta* in press. DOI: doi:10.1016/j.gca.2016.01.018.
- 1059
- 1060

1061 **Figure captions**

1062 **Figure 1.** (A) Location map with the 2015 Extended Ellett Line (EEL) stations in black dots. Deep,  
 1063 ocean currents are indicated by black arrows (below the pycnocline). The cold overflow currents are  
 1064 shown by blue arrows. Dotted lines represent intermittent currents. Orange and yellow lines reflect the  
 1065 warm surface waters. The locations of the Faroe-Shetland Channel (FSC), Faroe Bank Channel (FBC)  
 1066 and Wyville Thomson Ridge (WTR) are shown. For reference in the discussion, also shown are the  
 1067 locations of Station 23 in the FSC (yellow square; Lacan and Jeandel 2004b) and Stations 15.5 and  
 1068 17.5 in the Labrador Sea (green squares; Filippova et al. 2017). (B) Detailed view of the 2015 EEL  
 1069 stations, with those sampled in this study highlighted by large labelled symbols (blue, red, grey). *Water*  
 1070 *masses*: DWBC – Deep Western Boundary Current, LSW – Labrador Sea Water, ISOW – Iceland-  
 1071 Scotland Overflow Water, DSO – Denmark Strait Overflow, NAC - North Atlantic Current, WNAW -  
 1072 Western North Atlantic Water, ENAW - Eastern North Atlantic Water. *Ocean basins*: LS – Labrador  
 1073 Sea, IB – Iceland Basin, IS – Irminger Sea, RHP – Rockall-Hatton Plateau, RT – Rockall Trough, NS  
 1074 – Norwegian Sea. The figure was created using ODV software, available at  
 1075 <https://odv.awi.de/en/home/> (Schlitzer 2016). (For interpretation of the references to colour in this and  
 1076 other figures herein, the reader is referred to the electronic version of this article.)

1077 **Figure 2.** Sections of: (A) temperature (°C), (B) salinity, (C) potential density  $\sigma_\theta$  (kg/m<sup>3</sup>), (D) dissolved  
 1078 oxygen ( $\mu\text{mol/kg}$ ), (E) silica ( $\mu\text{mol/kg}$ ), (F) phosphate ( $\mu\text{mol/kg}$ ). The potential density section has  
 1079 contours delineating the ranges identified by Holliday et al. (2015) as representative of different water  
 1080 masses, with acronyms identifying the dominant water mass (see Figure 1 caption for acronyms). The  
 1081 data are from 920 bottle samples (black dots) collected from 85 stations over ~1300 km of cruise track  
 1082 during the 2015 EEL campaign. The figure was created using ODV software, available at  
 1083 <https://odv.awi.de/en/home/> (Schlitzer 2016).

1084 **Figure 3.** (A) Depth (m) vs. potential temperature (°C), (B) depth (m) vs. salinity, (C) potential  
 1085 temperature (°C) vs. salinity with the isopycnals defined by the grey lines, for the open ocean stations  
 1086 in this study during the 2015 EEL. The bottle data are indicated by symbols that correspond to those  
 1087 on the location map (Figure 1), superimposed on the CTD data. Small discrepancies between CTD and  
 1088 bottle data arise due to CTD data collection on the downcast and bottle data collection on the up-cast.  
 1089 The depths of the deepest samples at IB16 are indicated in (C) with reference to Section 4.1. The figure  
 1090 was created using ODV software, available at <https://odv.awi.de/en/home/> (Schlitzer 2016).

1091 **Figure 4.** Concentration-depth profiles of selected REE to span the light (Nd), middle (Dy) and heavy  
 1092 (Yb) range. All concentrations are in pmol/kg. Error bars represent  $2\sigma$  uncertainty from repeat  
 1093 measurement of the BATS 2000 m reference seawater during the study (Table 2). To note, surface  
 1094 waters from O and all 9G samples were not filtered.

1095 **Figure 5.** REE concentrations normalised to the Post-Archaean Australian Shale (PAAS) values of  
 1096 Taylor and McLennan (1985) as presented in Freslon et al. (2014). The BATS 2000 m pattern (van de  
 1097 Flierdt et al. 2012) is shown for comparison in each panel (bold red line). To note, surface waters from  
 1098 O and all 9G samples were not filtered.

1099 **Figure 6.** Normalisation by pISOW of (A-E) the 5 open ocean stations along the EEL and (F) DLSW  
 1100 and BATS 2000 m. Normalisation by DLSW of (G-K) the 5 open ocean EEL stations and (L) pISOW  
 1101 and BATS 2000 m. The error bars shown in (A-F) represent the combined 2SD from normalisation of  
 1102 IB16 (1550 m, shown in F) by pISOW, and in (G-L) are based on the combined 2SD from  
 1103 normalisation of F (1000-1499 m) by DSLW. The REE concentrations are from the literature: BATS

1104 2000 m (van de Flierdt et al. 2012), pISOW (Lacan and Jeandel 2004b), and deep (D)LSW (Filippova  
1105 et al. 2017).

1106 **Figure 7:** The water column increase of Nd concentrations at depth relative to the surface ocean  
1107 ( $[\text{Nd}]_{\text{depth}}/[\text{Nd}]_{\text{surface}}$ ) for the 5 open ocean stations, with comparison to selected stations in the Southern  
1108 Ocean in Hathorne et al. (2015).

1109 **Figure 8. (A)** The PAAS normalised REE concentrations presented as the MREE anomaly  
1110 ( $\text{MREE}/\text{MREE}^* = (\text{Gd}+\text{Tb}+\text{Dy})/[(\text{La}+\text{Pr}+\text{Nd}+\text{Tm}+\text{Yb}+\text{Lu})/2]$ ) vs. the HREE/LREE ratio  
1111 ( $[\text{Tm}+\text{Yb}+\text{Lu}]/[\text{La}+\text{Pr}+\text{Nd}]$ ). Sample depth presented as height above seafloor as a % of the water  
1112 column depth vs. **(B)** MREE/MREE\* and **(C)** HREE/LREE. The REE source data (large circles) are  
1113 collated REE concentrations representing different potential sources of REE in the marine  
1114 environment, both solid and aqueous phases: Bermuda Atlantic Time Series (BATS) reference  
1115 seawater from 15 m and 2000 m water depths (van de Flierdt et al. 2012), biogenic carbonate from  
1116 warm water corals in the North Atlantic (Sholkovitz and Shen 1995), marine sedimentary pore waters  
1117 collected in the Northeast Pacific along the Oregon margin, from cores in a depth transect (Abbott et  
1118 al. 2015b), labile Fe phases (Bayon et al. 2004, Gutjahr et al. 2007, Du et al. 2016), sedimentary organic  
1119 matter (Freslon et al. 2014), Icelandic ash (Tepe and Bau 2014). Details of average values used in this  
1120 study are in Table S3. The pore water data (Abbott et al., 2015b) represent the average REE  
1121 concentrations in pore waters of the top 5 cm of sediment from cores HH200, HH500, HH1200 and  
1122 HH3000, corresponding to water column depths of 202 m, 500 m, 1216 m, and 3060 m respectively.  
1123 The depth-related differences in pore water MREE/MREE\* and HREE/LREE are more clearly seen in  
1124 Figure 10. To note, surface waters from O and all 9G samples were not filtered.

1125 **Figure 9. (A)** “Excess”  $\text{REE}_N$  in the deepest seawater samples to identify the phase contributing excess  
1126 REE concentrations to the water column, calculated by subtracting the PAAS normalised REE in the  
1127 overlying sample from the deepest sample at each of the EEL stations ( $\text{REE}_N$  deepest sample –  $\text{REE}_N$   
1128 overlying sample). **(B)** Potential sources of REE to seawater. **(C)** The same as **Figure 8**, with the  
1129 addition of the REE composition (MREE/MREE\* vs. HREE/LREE) of the “excess” REE at stations  
1130 F, O, P, 9G, IB22/23. References listed in caption of **Figure 8**. To note, surface waters from O and all  
1131 9G samples were not filtered.

1132 **Figure 10.** Mixing plots of **(A)** MREE/MREE\* vs.  $1/\text{MREE}$ , and **(B)** HREE/LREE vs.  $1/\text{HREE}$ , to  
1133 highlight the combined effects of REE composition and concentration. The MREE/MREE\* and  
1134 HREE/LREE are calculated using PAAS normalised data, and the non-normalised concentrations are  
1135 used for  $1/\text{MREE}$  and  $1/\text{HREE}$  (pmol/kg). Data for BATS seawater (15 m and 2000 m) are from van  
1136 de Flierdt et al. (2012). The pore water data are from Abbott et al. (2015b) and represent the average  
1137 REE concentrations in pore waters of the top 5 cm of sediment from cores HH200, HH500, HH1200  
1138 and HH3000, corresponding to water column depths of 202 m, 500 m, 1216 m, and 3060 m  
1139 respectively. The shallowest and deepest cores are labelled in the figures, with the intervening cores  
1140 between these in depth order. Mixing lines are represented by dotted lines between BATS 15 m and  
1141 pore waters at 202 m depth, and BATS 2000 m and pore waters at 3060 m depth. The crosses on the  
1142 mixing lines represent pore water REE contributions of 2 %, 10 % and 25 % to BATS 15 m (HH200)  
1143 and BATS 2000 m (HH3000). The % contributions are labelled for mixing between BATS 15 m and  
1144 HH200 in the top panel only for clarity. To note, surface waters from O and all 9G samples were not  
1145 filtered.

1146 **Figure 11.** Depth variation of the nutrient concentrations ( $\mu\text{mol/kg}$ ) at the 5 open ocean stations in this  
1147 study. The lower panels show variation in Yb concentration ( $\text{pmol/kg}$ ) vs. each of the three nutrients  
1148 (phosphate, total nitrogen, silica).

1149 **Figure 12.** Depth variation of dissolved oxygen concentrations ( $\mu\text{mol/kg}$ ) at the 5 open ocean stations  
1150 in this study (left column). The apparent oxygen utilization (AOU;  $\mu\text{mol/kg}$ ) is also shown for  
1151 comparison (right column). Lower panels show nutrient concentrations (phosphate, total nitrogen,  
1152 silica) vs. dissolved oxygen and AOU ( $\mu\text{mol/kg}$ ) at the same stations. The open symbols represent  
1153 waters below the permanent pycnocline.

1154 **Figure 13.** Comparison of (A) the REE partitioning behaviour from water to bacteria, with (B) the  
1155 PAAS-normalised difference between ODZ and surface REE concentrations. For clarity, the 1SD  
1156 propagated errors are shown for station O data only. (C) The PAAS-normalised distribution profiles  
1157 of F and O showing only the surface and ODZ data to highlight the lower REE concentrations in the  
1158 surface waters. The REE partitioning data in (A) are from Takahashi et al. (2005) and Takahashi et al.  
1159 (2007), from experiments carried out at pH 4 and  $I = 0.01 \text{ M NaCl}$ . To note, surface samples from O  
1160 were not filtered.

1161

1162

1163 **Tables**

1164 Table 1: Water mass properties of selected stations and depths along the EEL 2015 cruise, with  
1165 comparison to end-member water masses in published work.

1166

Water mass	Potential temp (°C)	Salinity	$\sigma\theta$ (kg/m <sup>3</sup> )	Oxygen (μmol/kg)	Silica (μmol/kg)	Phosphate (μmol/kg)	Total N (μmol/kg)	MREE/MREE* (a)	HREE/LREE (b)	Reference
<i>EEL 2015 stations:</i>										
ENAW (O, 149 m)	9.79	35.40	27.31	270.7	1.88	0.60	10.42	1.01	3.73	
WNAW (IB16, 351 m)	7.56	35.20	27.50	279.4	6.58	0.89	14.00	0.99	3.51	
LSW (F, 1000-1499 m)	4.22	34.98	27.77	261.0	11.20	1.13	16.87	0.89	4.15	
LSW (IB9, 1502 m)	3.84	34.92	27.76	269.3	11.76	1.08	17.09	0.87	3.93	
ISOW (IB16, 1550 m)	3.53	35.00	27.85	279.1	9.75	1.01	15.32	1.01	3.62	
ISOW (IB16, 1686 m)	3.10	35.00	27.89	280.4	10.17	1.03	15.67	1.06	3.34	
<i>Published work:</i>										
ISOW (Stn 23)	-0.35	34.89	28.03	440.66*				1.05	3.45	(1)
DLSW (Stns 15.5, 17.5)	3.49	34.92	27.77	264.42 <sup>§</sup>				0.89	3.86	(2)
BATS 2000 m								0.92	4.11	(3)

1167

1168 The PAAS normalised REE concentrations are presented as (a) the MREE anomaly  
1169 (MREE/MREE\*=(Gd+Tb+Dy)/[(La+Pr+Nd+Tm+Yb+Lu)/2])and (b) the HREE/LREE ratio  
1170 ([Tm+Yb+Lu]/[La+Pr+Nd]).

1171 References: (1) Lacan and Jeandel 2004; (2) Filippova et al. 2017; (3) van de Flierdt et al. 2012.

1172 \*Conversion from 10.14 ml/l

1173 §Conversion from 6.09 ml/l

1174

1175

1176 Table 2: Dissolved REE concentrations in reference samples measured during the course of this study:  
1177 consensus values of the GEOTRACES intercalibration seawater from the Bermuda time series station  
1178 (BATS) 2000 m (van de Flierdt et al. 2012); published values of Wang et al. 2014 for NASS-6  
1179 (National Research Council Canada) coastal seawater.

1180

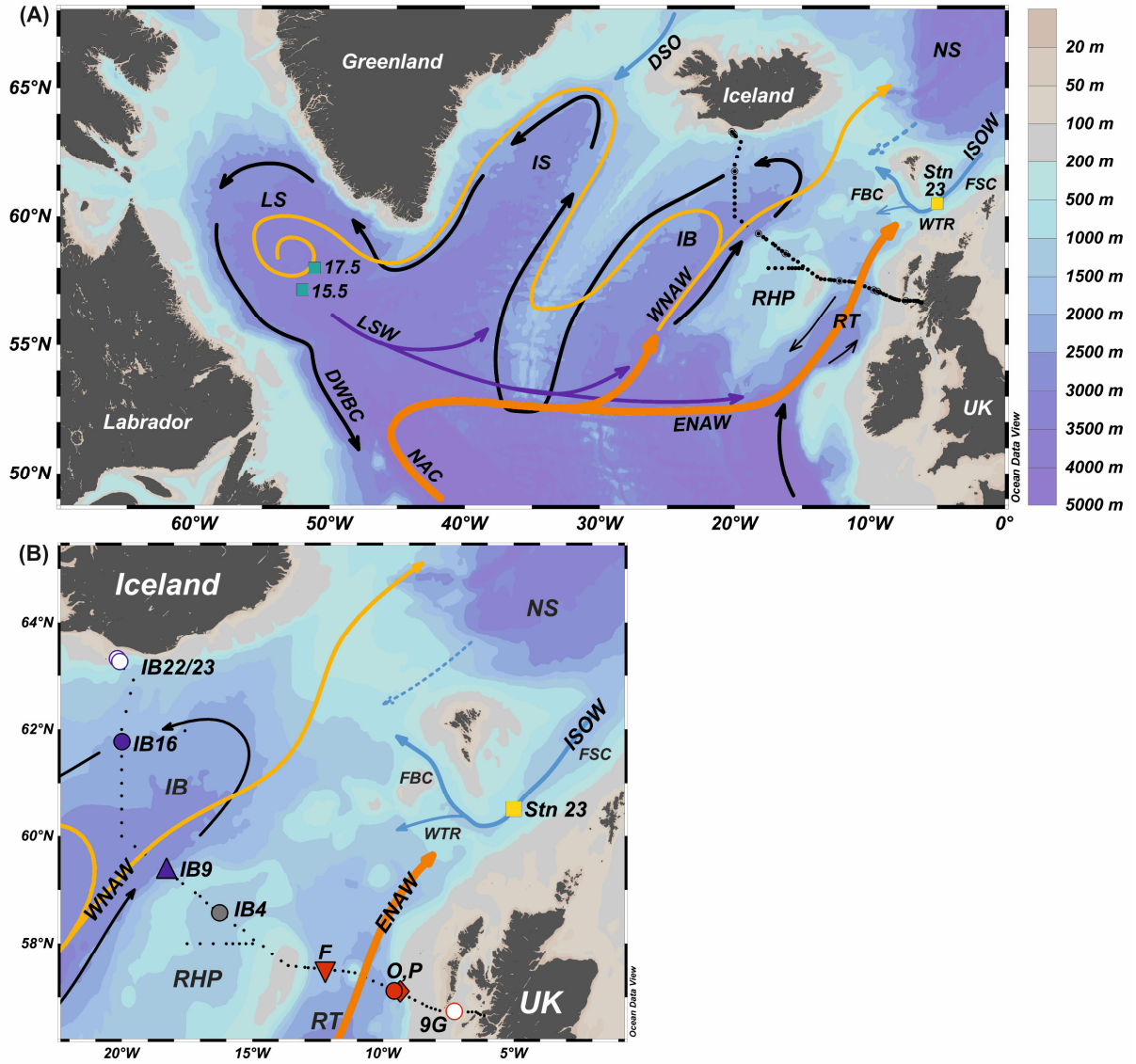
Element	La	Ce	Pr	Nd	Sm	Eu	Gd	Tb	Dy	Ho	Er	Tm	Yb	Lu	Y
<b>BATS 2000 m (n=19)</b>															
Mean concentration (pmol/kg)	<b>23.76</b>	<b>4.41</b>	<b>4.31</b>	<b>18.48</b>	<b>3.93</b>	<b>0.93</b>	<b>5.07</b>	<b>0.82</b>	<b>6.00</b>	<b>1.54</b>	<b>5.23</b>	<b>0.76</b>	<b>5.07</b>	<b>0.84</b>	<b>153</b>
2SD	2.05	0.55	0.31	1.14	0.62	0.13	0.55	0.09	0.58	0.14	0.50	0.08	0.52	0.09	14
2RSD (%)	9	12	7	6	16	14	11	10	10	9	10	10	10	10	9
Consensus values (pmol/kg)	23.61	5.12	4.03	17.33	3.45	0.91	4.84	0.79	5.780	1.52	5.04	0.75	4.76	0.81	
2SD of consensus values	2.79	2.27	0.35	1.22	0.354	0.10	0.53	0.08	0.38	0.09	0.25	0.05	0.25	0.04	
Deviation to consensus (%)	1	-14	7	7	14	2	5	4	3	1	4	2	6	4	
<b>NASS-6 (n=12)</b>															
Mean concentration (pmol/kg)	<b>72.15</b>	<b>28.71</b>	<b>10.76</b>	<b>45.50</b>	<b>8.05</b>	<b>1.59</b>	<b>9.74</b>	<b>1.39</b>	<b>9.81</b>	<b>2.39</b>	<b>8.01</b>	<b>1.12</b>	<b>7.74</b>	<b>1.26</b>	<b>229</b>
2SD	7.69	4.56	0.75	3.70	0.80	0.15	0.84	0.13	0.84	0.21	0.66	0.1	0.6	0.1	23
2RSD (%)	11	16	7	8	10	10	9	10	9	9	8	12	7	8	10
Published values (pmol/kg)	75.20	31.25	11.72	45.90	8.79	1.76	8.30	1.46	9.77	2.34	7.81	1.07	7.42	1.17	264
2SD of published values	8.79	5.86	1.95	7.81	0.98	0.20	1.76	0.59	0.98	0.68	0.98	0.29	1.56	0.39	39
Deviation to published (%)	-4	-8	-8	-1	-8	-9	17	-5	0	2	3	5	4	7	-13

1181

1182

1 Figure 1

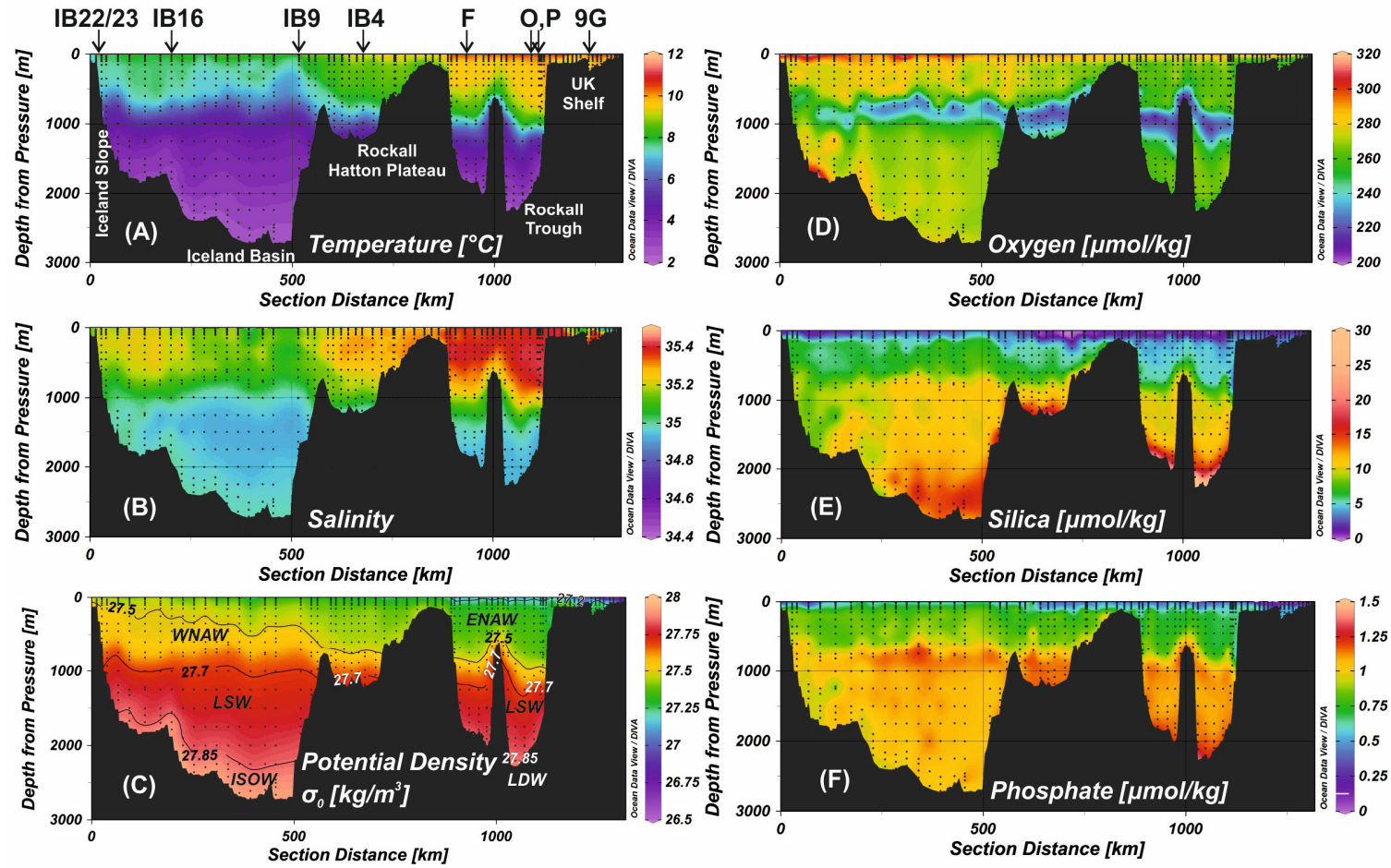
2



3

4

5 Error! Reference source not found.

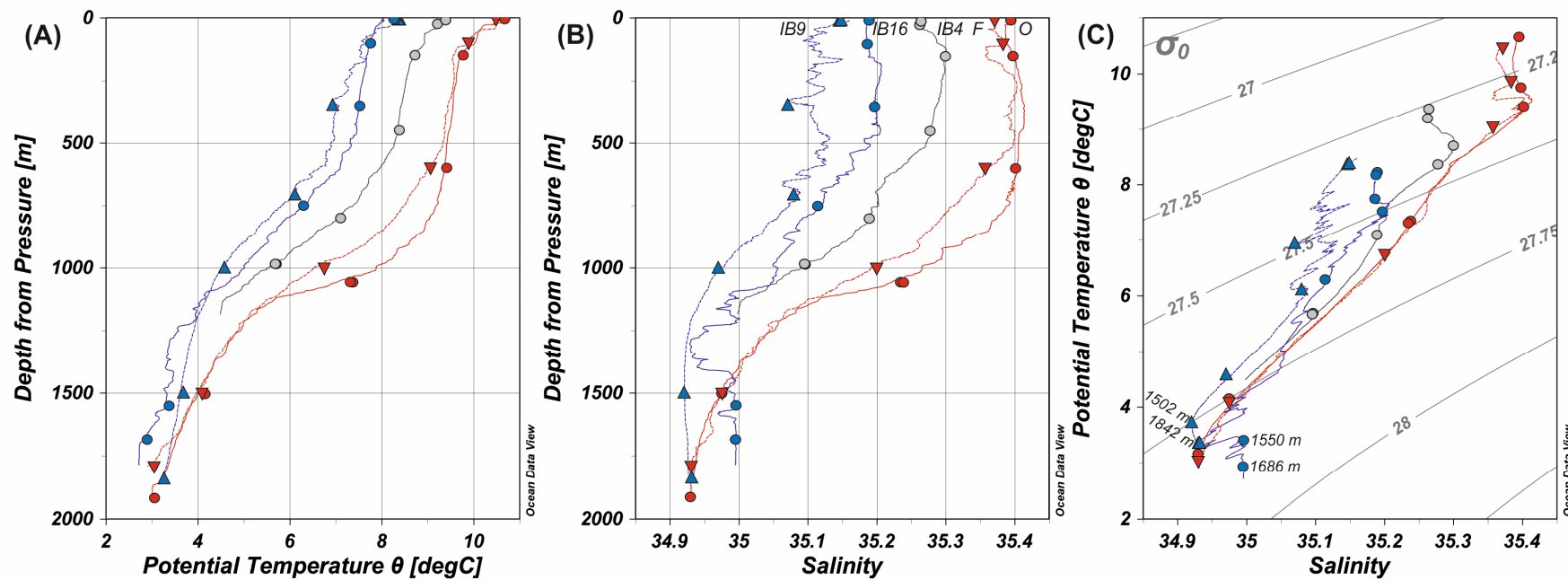


6

7

8 Error! Reference source not found.

9



10

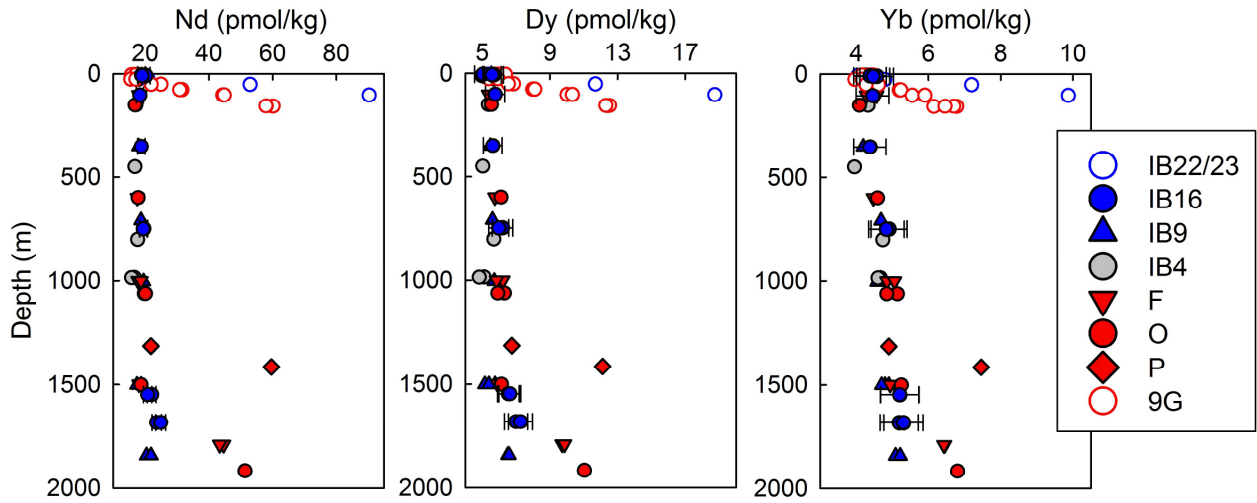
11

12

13

14 **Error! Reference source not found.**

15

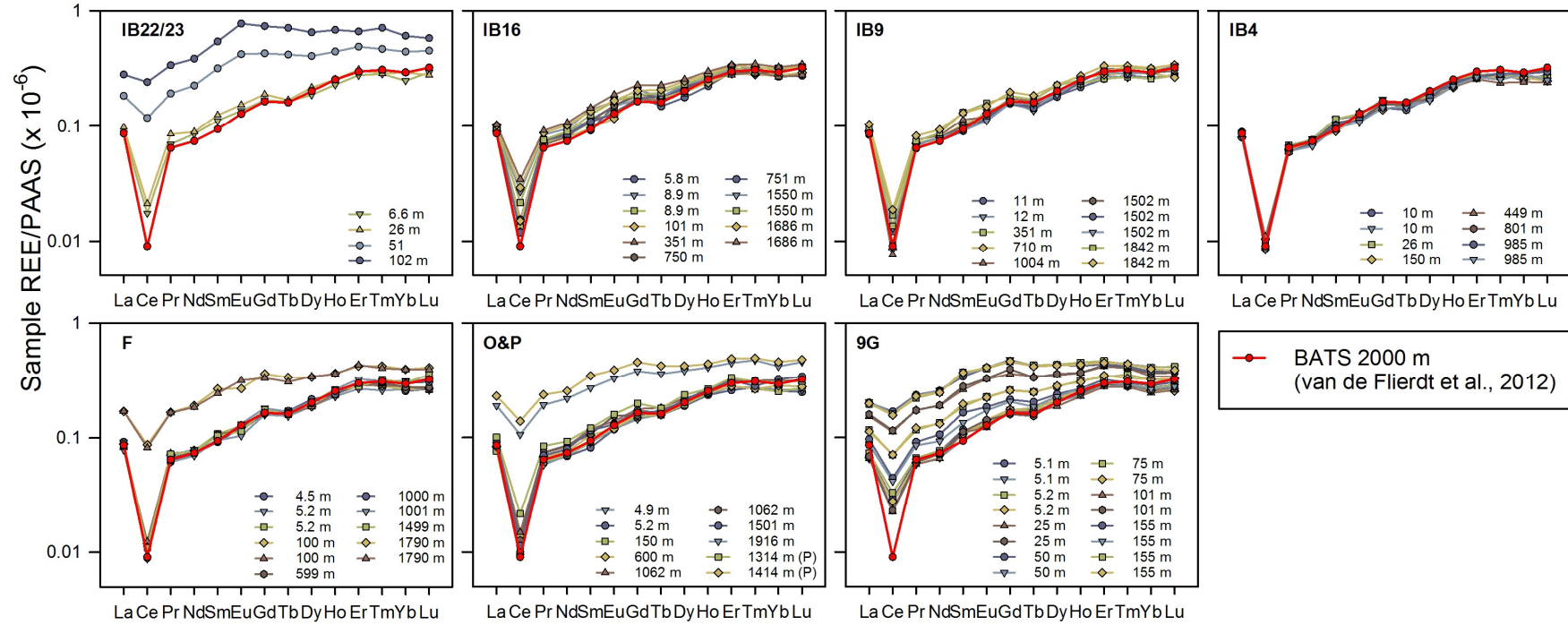


16

17

18 **Error! Reference source not found.**

19



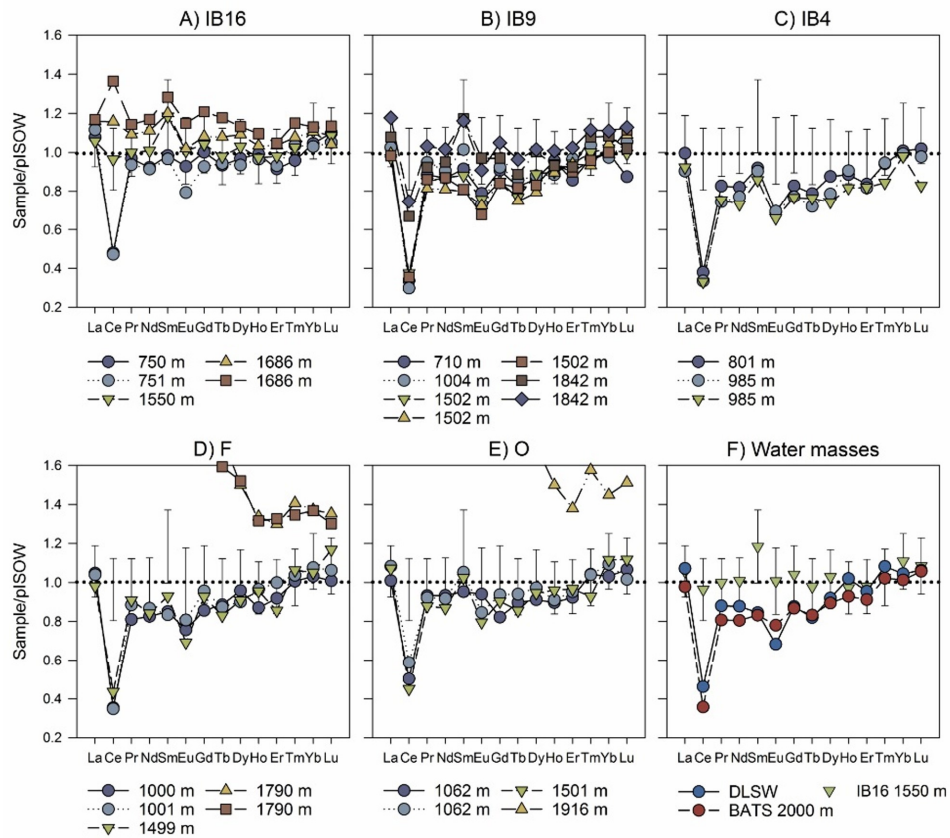
20

21

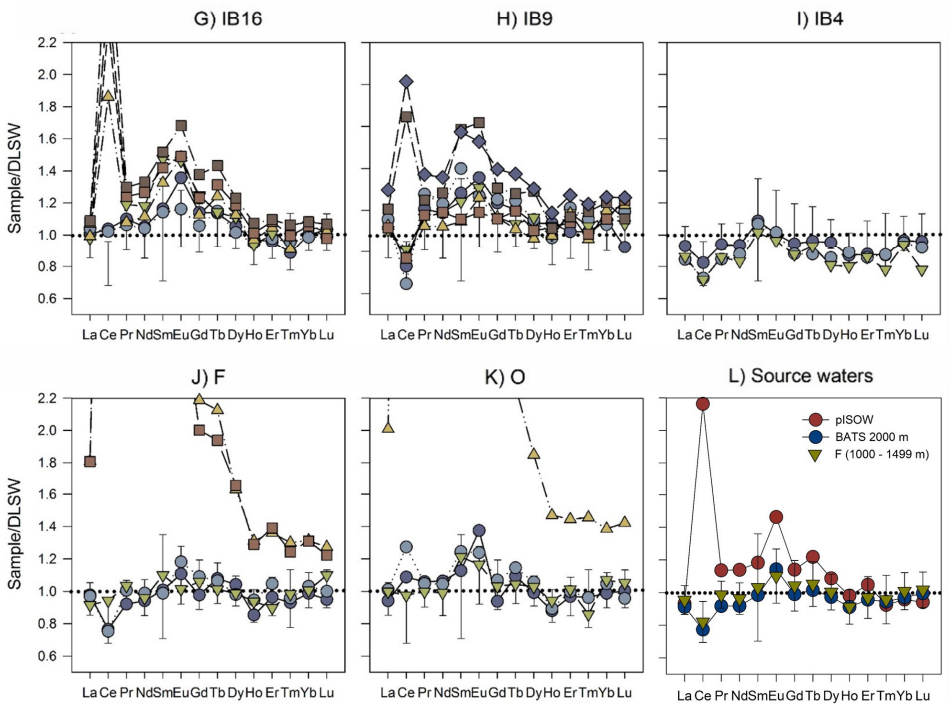
22

23 **Error! Reference source not found.**

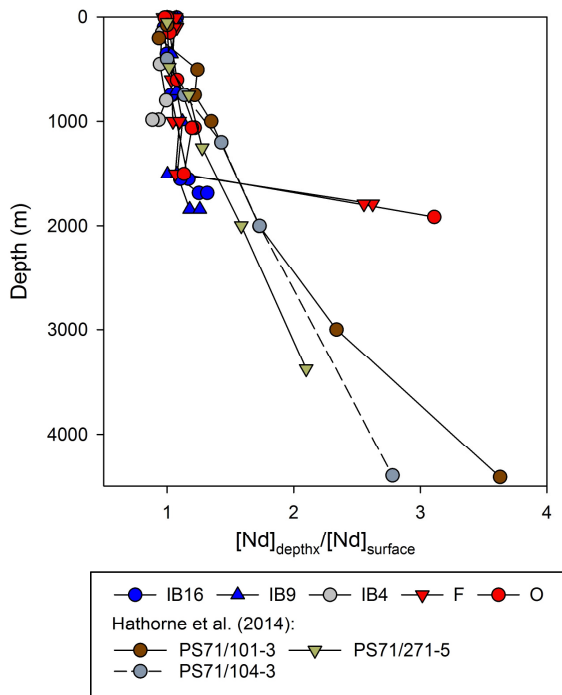
Normalised to pISOW



Normalised to DLSW



25 **Error! Reference source not found.**

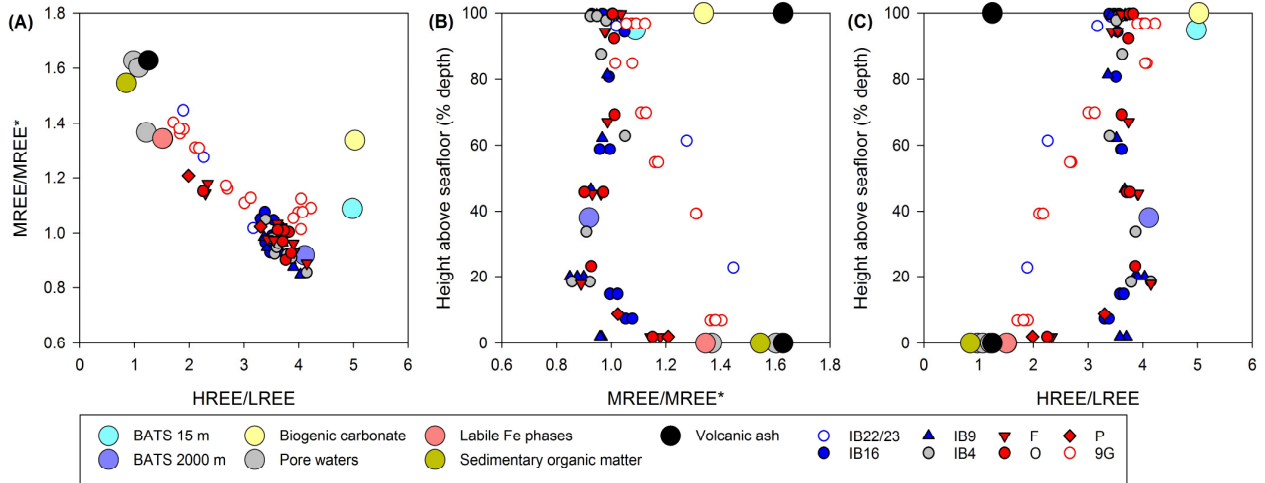


26

27

28 **Error! Reference source not found.**

29



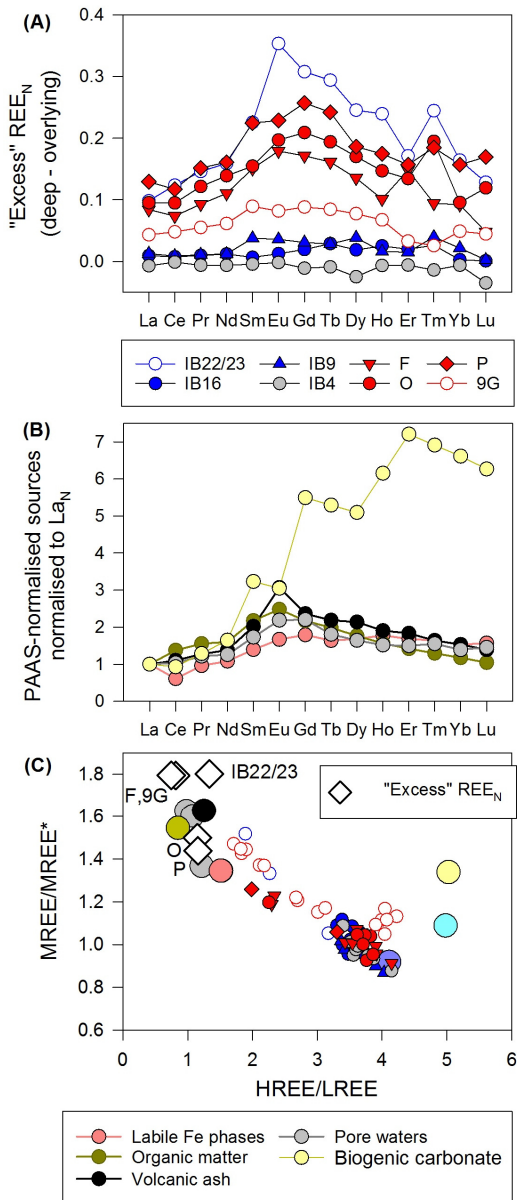
30

31

32

33 Error! Reference source not found.

34

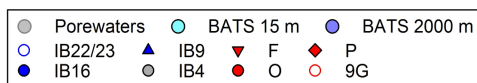
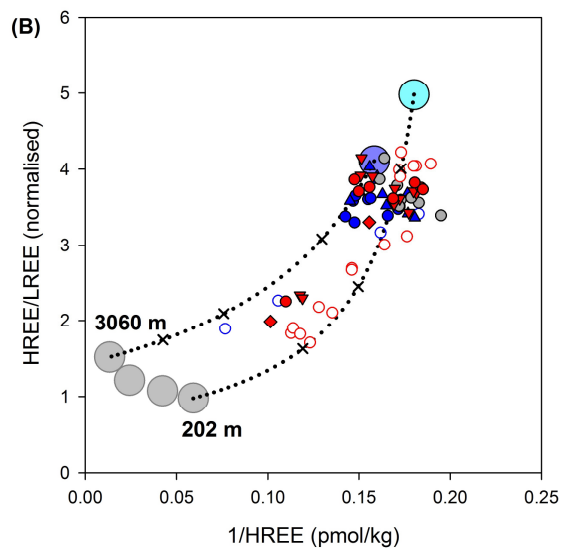
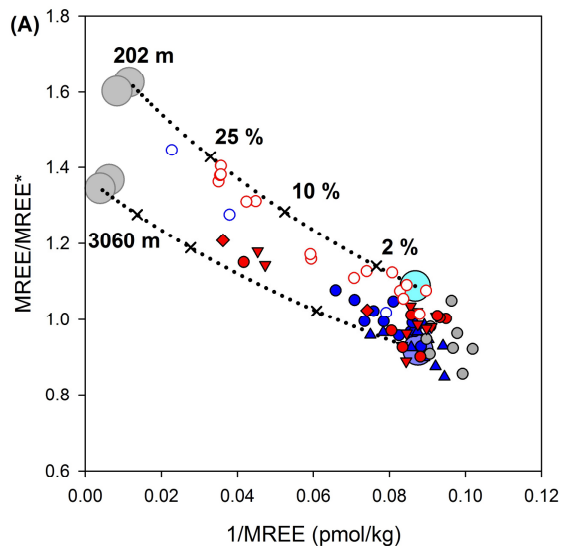


35

36

37

38 **Error! Reference source not found.**



39

40

41

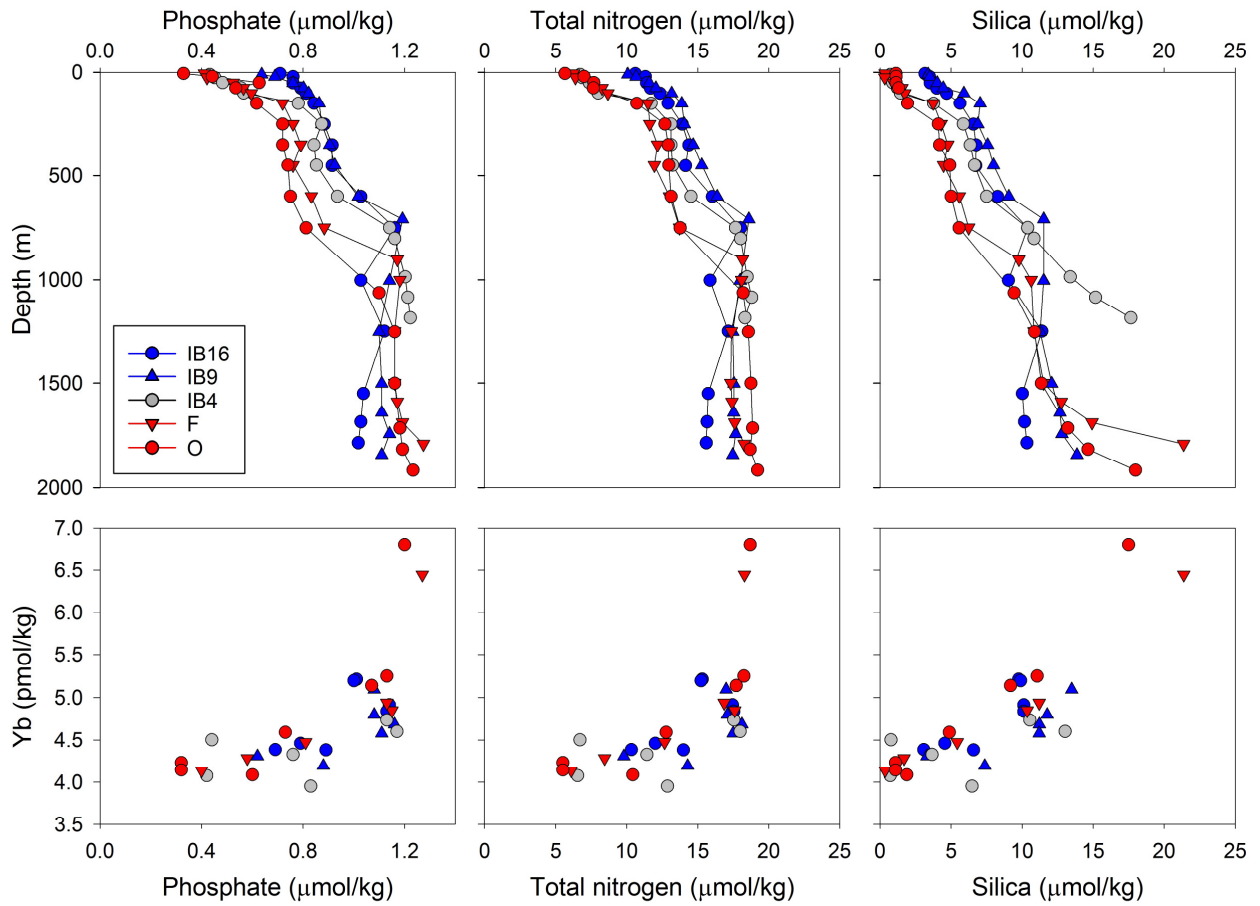
42 —

43

44

45

46

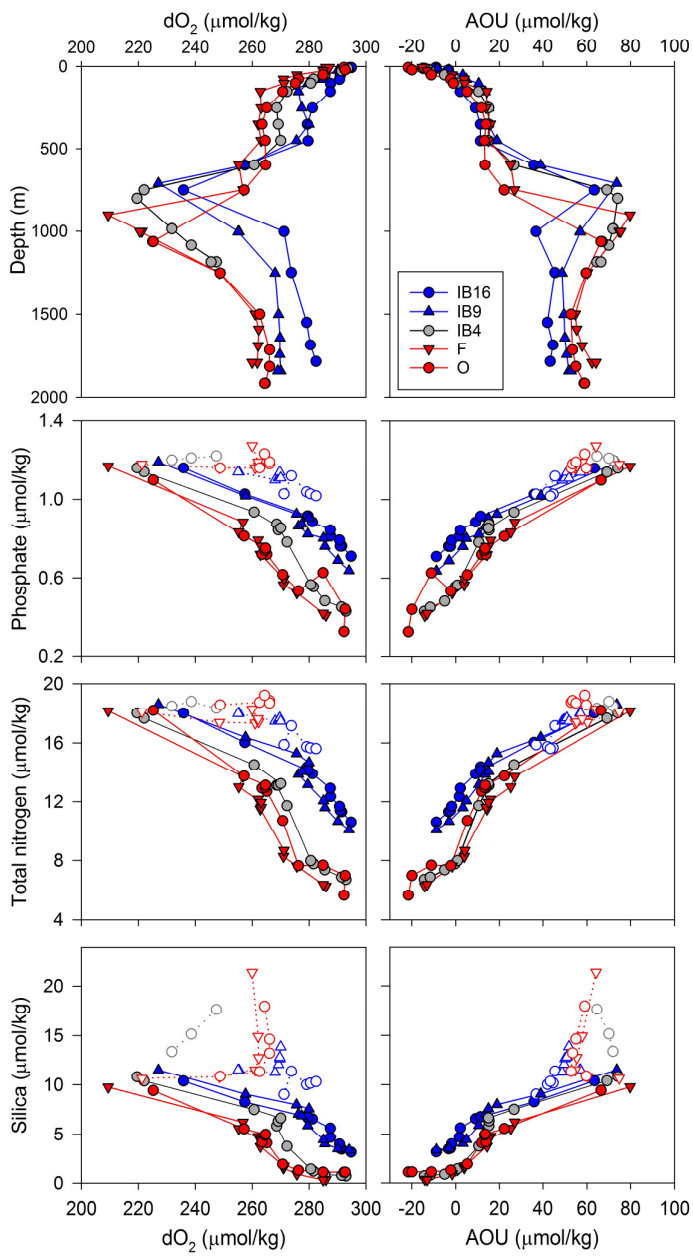


47

48

49

50 Error! Reference source not found.



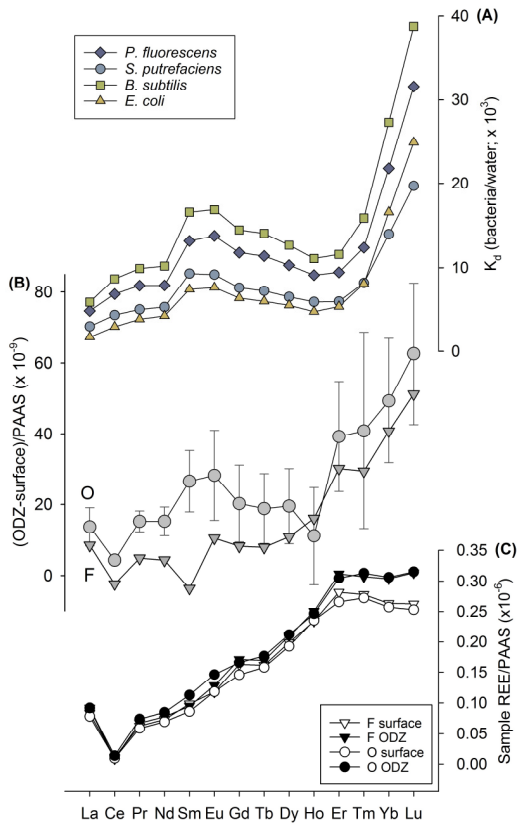
51

52

53

54 Error! Reference source not found.

55



56

57

58